

Perspectives for Applications of Quantum Imaging

Marta Gilaberte Basset, Frank Setzpfandt, Fabian Steinlechner, Erik Beckert, Thomas Pertsch, and Markus Gräfe*

Quantum imaging is a multifaceted field of research that promises highly efficient imaging in extreme spectral ranges as well as ultralow-light microscopy. Since the first proof-of-concept experiments over 30 years ago, the field has evolved from highly fascinating academic research to the verge of demonstrating practical technological enhancements in imaging and microscopy. Here, the aim is to give researchers from outside the quantum optical community, in particular those applying imaging technology, an overview of several promising quantum imaging approaches and evaluate both the quantum benefit and the prospects for practical usage in the near future. Several use case scenarios are discussed and a careful analysis of related technology requirements and necessary developments toward practical and commercial application is provided.

1. Introduction

Optical microscopy and spectroscopy are major tools in modern research covering various disciplines, ranging from fundamental physics, to material science, chemistry, and life sciences. It is very interesting to see how new knowledge about the nature of light has led to new imaging applications throughout history. The most simplified description of light is given by considering it as ray bundles (“Strahlenbündel”). This geometric optics picture allows the description of the working principle of lenses and their application in form of, for example, magnification glasses. However, taking the wave nature of light into account allows to

understand diffraction and interference. This finds application for instance in interference microscopes. Inevitably linked to this insight is that the resolution of an optical system depends linearly on the wavelength of the light used for observation. The fundamental insight that light exists in form of discrete energy portions—quanta—started the so-called first quantum revolution at the beginning of the twentieth century. It is the basis of the whole photonics and laser industry. Moreover, without this finding fluorescence microscopy, a versatile and widespread tool in modern life science, cannot be explained. Today, we are witnessing the second quantum revolution,

where *quantum states*, which can exhibit superposition and entanglement, are harnessed for quantum technological applications. This new insights make various novel imaging modalities possible.

Breaking the limitations of today’s established imaging schemes is a goal many researcher try to realize all around the globe. This addresses resolution, SNR, contrast, and spectral range. Exploiting the quantum properties of light is one way to overcome some of those limitations. In doing so, entanglement plays a central role. In particular, momentum-, energy-, and position correlations of entangled photon pairs are crucial.^[1,2] They allow for spectroscopy and imaging in spectral ranges where no efficient detection is possible or even imaging with light that actually never interacted with a sample.^[3–6] Furthermore, by utilizing certain quantum states of light and their photon number statistics, sensing and imaging beyond classical limitations, like the shot noise level, become possible.^[7–13] Additionally, two-photon fluorescence microscopy can be carried out at extreme low light intensity when applying quantum light, enabling new insights into photosensitive biochemical probes.^[14]

In essence, many quantum-enhanced imaging schemes harness the beneficial properties of correlated photon pairs. Here, we want to give a review on different imaging methodologies based on photon pairs. First, in Section 2, we give a brief overview of the basic properties of various quantum states of light and point out the special properties of photon pairs and related states. Furthermore, we describe how photon pairs are commonly generated and how their properties can be linked to the generation. Photon pairs can be used for imaging in various ways, where the photons are employed in fundamentally different manners. We organize our review of imaging methods according to how many of the photons interact with the object and are used for recording an image. **Figure 1** sketches the three main categories

M. Gilaberte Basset, Dr. F. Steinlechner, E. Beckert, Prof. T. Pertsch, Dr. M. Gräfe

Fraunhofer Institute of Applied Optics and Precision Engineering IOF Jena

Albert-Einstein-Straße 7, 07745 Jena, Germany

E-mail: markus.graefe@iof.fraunhofer.de


Dr. F. Setzpfandt, Dr. F. Steinlechner, Prof. T. Pertsch

Institute of Applied Physics

Abbe Center of Photonics

Friedrich-Schiller-Universität Jena

Albert-Einstein-Straße 15, 07745 Jena, Germany

 The ORCID identification number(s) for the author(s) of this article can be found under <https://doi.org/10.1002/lpor.201900097>

Copyright 2019, Fraunhofer Institute for Applied Optics and Precision Engineering IOF. Published by WILEY-VCH Verlag GmbH & Co. KGaA, Weinheim. This is an open access article under the terms of the Creative Commons Attribution License, which permits use, distribution and reproduction in any medium, provided the original work is properly cited.

The copyright line for this article was changed on October 1, 2019 after original online publication.

DOI: 10.1002/lpor.201900097

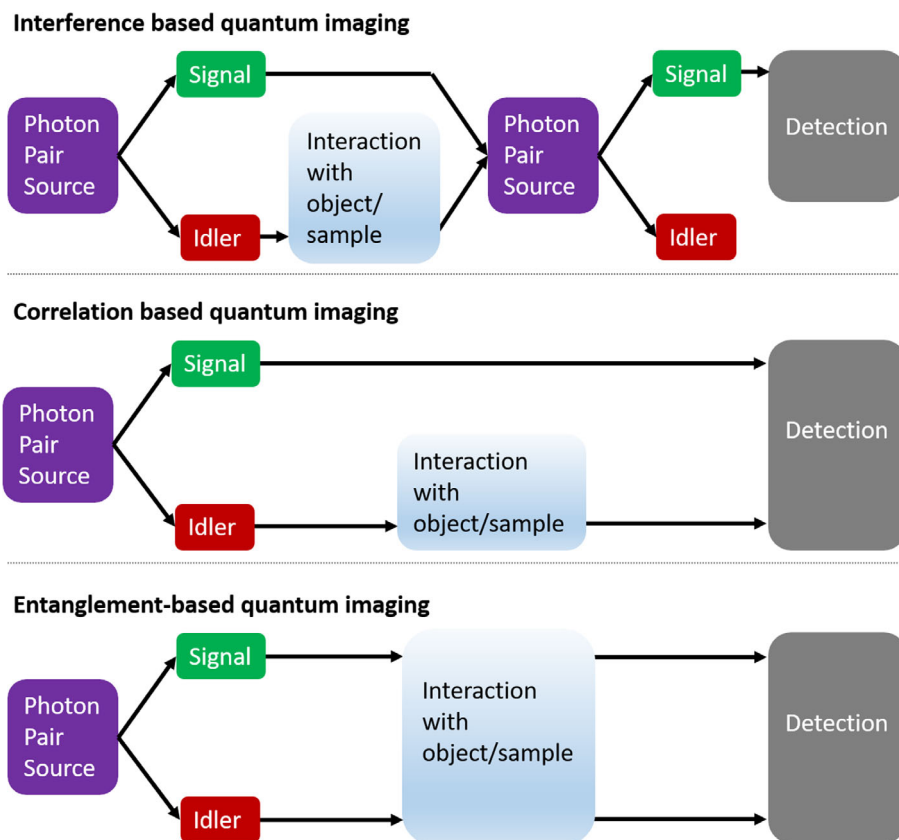


Figure 1. Schematic overview to categorize the quantum imaging approaches into three groups.

for quantum imaging techniques we define for systematization. Quantum imaging methods, where only one photon of the pair interacts with the sample and its partner is used for the actual measurements are discussed in Section 3. Here, the image formation is based on quantum interference of several sources. In contrast to this, the approaches covered in Section 4 still have only one photon of the pair interacting with the sample, but both are needed to form an image utilizing their intrinsic correlations. Finally, methods where the whole pair interacts with the object and is detected or stimulates detectable fluorescence light are described in Section 5. These approaches make use of entanglement of the photon pairs. A direct comparison to standard microscopy techniques like phase contrast microscopy or laser scanning microscopy can be drawn.

Some of the described imaging approaches are based on spatial correlations between the two photons of a pair induced in the generation process. As similar correlations are also present in the spectrum of the photon pairs, equivalent methods for quantum-enhanced spectroscopy have been developed, which will be also described herein.

Basically all of the described methods up to now have been only fundamentally investigated but not yet used in real-world applications. Therefore, in our discussion we will highlight their particular advantages and potential applications where these advantages would be of relevance. Furthermore, key experimental challenges will be mentioned that have to be resolved in order to foster application of the described methods. These often are related to the properties of the used quantum light source or

detection hardware. To enable an assessment of the state of the art in these fields with respect to the challenges connected to implementing quantum imaging schemes, we also will give a brief overview over different source and detector implementations in Section 6.

In addition, we would like to mention several review papers and overview articles covering topics that are touched on here but are beyond the scope of this review: single photon sources and detectors,^[15–17] integrated-optical sources of entangled photons,^[18,19] and generation of photon pairs via spontaneous four wave mixing.^[20–22]

2. Fundamentals

Taking the quantum nature of light into account, it becomes possible to envision new imaging schemes, which may be realized in actual quantum-enhanced microscopes or imaging devices. This article briefly explains those non-classical properties or phenomena associated with quantum light that directly give rise to applications within the field of quantum-enhanced imaging.

2.1. Photon Number Statistics

As all possible states of light can be described within quantum optics, first we want to define which types of states we are considering here when we describe modalities for quantum-enhanced imaging. A practical way to distinguish different types of light

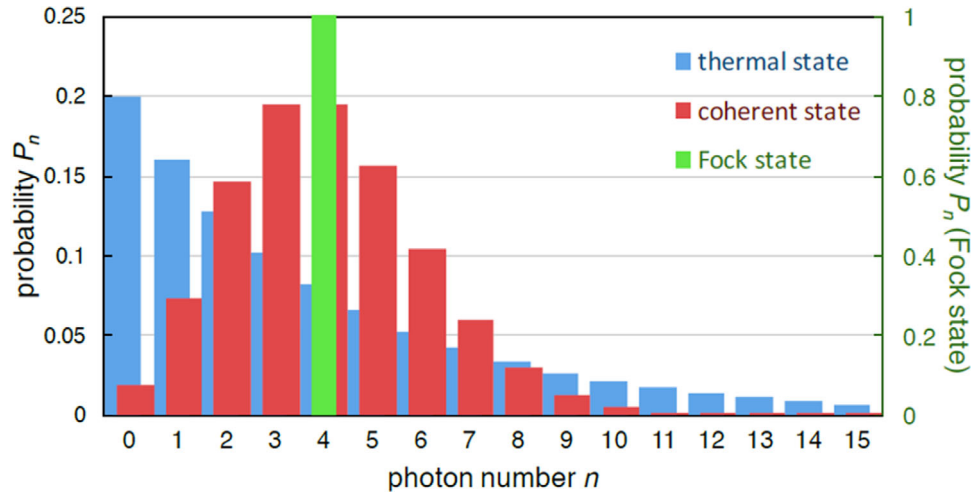


Figure 2. Photon number statistics for different quantum states of light: a thermal state (classical), a coherent state, and a Fock state (nonclassical). The mean photon number $\langle n \rangle = 4$ is identical for all three states. The right vertical axis applies to the Fock state distribution only.

is by means of their photon number statistics. Any given state of light can be characterized by its mean photon number $\langle \hat{n} \rangle$ and its variance $\langle (\Delta \hat{n})^2 \rangle$, where we first consider only a single spatial mode. While classical light is associated with a super-Poissonian distribution with $\langle (\Delta \hat{n})^2 \rangle > \langle \hat{n} \rangle$, non-classical light, which can only be described using quantum optics, is linked with a sub-Poissonian one, that is, $\langle (\Delta \hat{n})^2 \rangle < \langle \hat{n} \rangle$.^[7,9] An example for classical light is thermal radiation of a light bulb ($\langle (\Delta \hat{n})^2 \rangle = \langle \hat{n} \rangle + \langle \hat{n} \rangle^2$) and for non-classical light the Fock (photon number) states ($\langle (\Delta \hat{n})^2 \rangle = 0$). Coherent states, to which laser radiation can be often approximated to, lie exactly on the boundary with a Poissonian photon number statistics $\langle (\Delta \hat{n})^2 \rangle = \langle \hat{n} \rangle$.^[7,9] The different statistics are exemplarily shown in **Figure 2**, where we plot the photon number distributions for different types of light described by the same average photon number, that is, intensity. A measure for the non-classicality can be found by the so-called Mandel parameter^[23]:

$$Q_M = \frac{\langle (\Delta \hat{n})^2 \rangle}{\langle \hat{n} \rangle} - 1 \begin{cases} > 0 & \text{super-Poissonian (classical)} \\ = 0 & \text{Poissonian (coherent state)} \\ < 0 & \text{sub-Poissonian (non-classical)} \end{cases} \quad (1)$$

In essence, non-classical quantum states of light can show much lower fluctuations in their photon number, which could be utilized for enhanced SNR imaging. Here, we will consider imaging modalities that use photon pairs, states of light with exactly two photons and vanishing variance $\langle (\Delta \hat{n})^2 \rangle = 0$ as input. This entails the already-mentioned single-mode number states of light with $n = 2$, but is not limited to these basic states of light when several optical modes are considered. For multiple optical modes, the total photon number is described by the operator $\hat{N} = \sum_l \hat{n}_l$, with \hat{n}_l being the photon number in mode l . For multimode states, we will consider states where the variance of the total photon number $\langle (\Delta \hat{N})^2 \rangle = 0$. However, the photon numbers in the individual modes can have a non-zero variance in this case, giving rise to a variety of different states. In particular, this encompasses entangled states, which are the cornerstones of many applications of quantum optics,

like quantum computing and cryptography, and can also be beneficial in quantum-enhanced imaging. It is worth to mention here, that for two-mode photon-pair states it holds for signal (s) and idler (i) $\Delta(\hat{n}_s - \hat{n}_i) = 0$, which is caused by their mutual correlation.

A particular example of non-classical states not considered here are squeezed states of light.^[7,9] They also feature a sub-Poissonian statistics, offering the possibility for measurements with enhanced precision, which has been employed, for example, for subshot noise phase measurements in gravitational wave detectors.^[11–13]

2.2. Spontaneous Parametric Downconversion

The past two decades have seen a flurry of research dedicated to the generation and control of quantum states of light.

In particular, envisaged applications in photonic quantum computing and quantum networks have motivated significant efforts toward developing deterministic single-photon emitters—ideal photon guns.^[24] Technologies ranging from quantum dots and defects in solids to 2D materials, to atoms and ions are steadily improving in performance and have demonstrated that on-demand generation of pure single-photon Fock states is well within reach.

In the context of quantum imaging, deterministically triggering particular photon numbers is desirable but by no means a strict necessity and many quantum imaging protocols may also be implemented with probabilistic emission (typically a thermal photon number distribution). In quantum imaging, the ability to engineer the spatial and spectral properties of the emitted radiation over a potentially broad range of modes can be more decisive. As a result of decades of nonlinear optics research, photon sources based on parametric optical processes in nonlinear materials allow the highest level of control over spatial and spectral properties of the emitted radiation. This has resulted in a plethora of nonlinear-optics based sources of correlated, and even spatially entangled photons.

To date, the most widely used approach to generate photon pairs is based on spontaneous parametric downconversion (SPDC) in second-order nonlinear crystals such as bismuth borate (BBO),^[25–29] lithium borate (LBO),^[30] lithium niobate (LN),^[31–33] and potassium titanyl phosphate (KTP).^[34–39] In the SPDC process, a strong pump field with frequency ω_p generates a spontaneous nonlinear polarization response in a nonlinear material, which may spontaneously result in the emission of a pair of lower-energy photons, commonly referred to as signal (at ω_s) and idler (at ω_i), where

$$\omega_p = \omega_i + \omega_s \quad (2)$$

due to energy conservation. For the pair generation process to be efficient, photon pairs generated in different regions of the nonlinear material must interfere constructively. This can be ensured by fulfilling the phase-matching condition for the propagation constants \mathbf{k} of the interacting waves,

$$\Delta\mathbf{k} = \mathbf{k}(\omega_s) + \mathbf{k}(\omega_i) - \mathbf{k}(\omega_p) = 0 \quad (3)$$

where $\Delta\mathbf{k}$ is called the phase mismatch and $|\mathbf{k}(\omega)| = 2\pi n(\omega)/\lambda$. Phrased, entirely equivalently, in terms of the three photon interaction, the phase-matching condition for the wave vectors simply reflects the conservation of total momentum in the SPDC process, $\mathbf{k}_s + \mathbf{k}_i = \mathbf{k}_p$.

The phase matching condition is usually not automatically fulfilled (i.e., or $\Delta\mathbf{k} \neq 0$) due to material dispersion, so that destructive interference occurs after propagation over a distance $\delta_c = 2\pi/\Delta k$, so that no photon pairs are generated.

In anisotropic nonlinear crystals, the phase mismatch can be compensated using the material's birefringence. This technique, known as birefringent phase matching (BPM) requires at least one of the SPDC photons to be polarized orthogonally with respect to the pump field, resulting in two distinct polarization configurations in BPM.^[40] The configuration in which one of the SPDC photons, for example, the idler, is co-polarized with respect to the pump is referred to as type-II BPM,^[25] whereas type-I BPM refers to the case in which the signal and idler are co-polarized.^[26] In general, BPM is achieved by angle tuning the crystal, which restricts the nonlinear material coefficients that can be exploited as well as the possible propagation geometries. Collinear geometries, in which all fields propagate along the same axis, are particularly desirable since they maximize the spatial overlap of the interacting fields and, as a consequence, increase the SPDC efficiency.^[27,29] However, since BPM involves at least one photon of extraordinary polarization, Poynting vector walk-off imposes limits to the useful crystal length.

An alternative approach is based on the ability to modulate the nonlinearity of ferroelectric crystals (e.g., via application of high-voltage field to patterned electrodes). In periodically poled nonlinear crystals (e.g., ppLN or ppKTP), the nonlinear polarization response is inverted periodically after a distance $\delta_c/2$, so that energy is continuously transferred from the pump to the downconverted fields. This approach, the so-called quasi-phase matching (QPM), allows for SPDC at almost arbitrary wavelength combinations and the otherwise impossible type-0 interaction where pump, signal, and idler photons are all co-polarized.^[32,34–38] However, when the *natural* phase-mismatch of the interaction is sig-

nificant, the required poling period may be prohibitively small from an engineering perspective. When this is the case, quasi-phase matching may still occur at odd multiples (phase-matching order m) of the poling period at the cost of reduced efficiency $\propto 1/m^2$. Another very beneficial feature of QPM is that it can be tailored such that all fields propagate along a principal axis of the nonlinear crystal. The absence of transverse spatial walk-off in this so-called non-critical phase-matching configuration enables efficient use of long nonlinear crystals and waveguide structures. Photon sources based on type-0 SPDC have resulted in some of the highest pair emission rates reported to date.^[41]

2.3. Photon-Pair Correlations

The ability to tailor the spectral and spatial properties of photons has led to remarkable progress in our understanding of quantum physics as well as applications in quantum information processing.^[42,43] Controlling the spatial and spectral correlations of two-photon states to the requirements of particular applications has been the topic of many theoretical and experimental works. In this section, we introduce some of the key spatial properties of photon pairs produced via SPDC in homogeneous nonlinear crystals. A detailed account of the underlying theory is beyond the scope of this review and we refer the reader to refs. [44–47] for an extensive introduction to transverse SPDC correlations, to refs. [44,48] for a more extensive background on the modal decomposition of SPDC states, and to refs. [49–52] for studies related to efficient fiber-coupling of photon pairs. We note, that photon pairs with tailored properties can also be generated in waveguide structures.^[18,19] However, as these have up to now not been used for quantum imaging, we will restrict our discussion to bulk nonlinear crystals.

Following the notation introduced in refs. [44,45], we assume that the SPDC emission is mainly directed along some preferential propagation axis (e.g., the z -axis). In this case, it is convenient to decompose the wave vectors of the three fields into a transverse component perpendicular to the propagation axis $\mathbf{q} = (k^x, k^y)$ and a longitudinal component $k^z(\mathbf{q}, \omega)$. To facilitate the separation of the signal and idler photons, the poling period of the nonlinear crystal is chosen to fulfill a quasi-collinear type-II QPM condition at center frequencies ω_s^0 and ω_i^0 and linear horizontal (H) and linear vertical (V) polarization states. Noting that spectral correlations of biphotons, which determine the properties such as coherence and correlation times, play a role in all experiments with photon pairs, we will focus only on the spatial properties of the SPDC state. Experimentally, such a situation can be achieved by placing spectral filters after the nonlinear crystal to restrict the detection bandwidth to a narrow range of frequencies. Under these assumption, we can express the leading terms of the state generated by SPDC emission as

$$|\Psi\rangle = |vac\rangle + \sqrt{\gamma} \int d\mathbf{q}_s d\mathbf{q}_i \Phi(\mathbf{q}_s, \mathbf{q}_i) |q_s\rangle_H |q_i\rangle_V + o(\gamma) \quad (4)$$

Here, γ indicates the photon-emission efficiency, which depends on the pump power and the nonlinear coefficient of the used nonlinear crystal, and $\Phi(\mathbf{q}_s, \mathbf{q}_i)$ denotes the normalized two-photon mode function in the transverse wave vector/momentum

domain.^[44,45,48,53,54] Typically, pump powers for SPDC are chosen such that $\gamma \ll 1$ and the higher-order terms denoted by $o(\gamma)$ in Equation (4) are negligible. Naturally, the vacuum contribution does not result in photon detection events and hence we consider only the spatial properties of the two-photon SPDC state in the following. Neglecting the effect of transverse spatial walk-off, and considering the typical experimental case where the pump is a Gaussian laser beam $E_p(\mathbf{q}) = [w_p/\sqrt{2\pi}] \exp(-|\mathbf{q}|^2 w_p^2/4)$ with the beam waist w_p located at the center of the nonlinear crystal of length L , we obtain the following closed form for the mode function^[44,48]:

$$\Phi(\mathbf{q}, \mathbf{q}') = K \exp\left(\frac{-|\mathbf{q} + \mathbf{q}'|^2 w_p^2}{4}\right) \text{sinc}\left(\frac{\Delta k(\mathbf{q}, \mathbf{q}')L}{2}\right) \quad (5)$$

where the proportionality constant K again depends on the pump power and the nonlinear coefficient of the nonlinear crystal to ensure proper normalization of the state Equation (4). From Equation (5), we see that the photon-pair mode function is determined by the interplay of the spatial properties of the pump beam and the phase matching function $\text{sinc}(x) = \sin(x)/x$ inside the nonlinear crystal. The transverse spatial bandwidth of the Gaussian pump beam determines the strength of transverse correlation, and the phase-matching bandwidth determines the single-photon bandwidth of the SPDC emission, which is generally is significantly larger than that of the pump field. We notice that the constraints imposed by energy conservation Equation (2) and phase-matching (momentum conservation) Equation (3) usually result in a non-separable two-photon mode function $\Phi(\mathbf{q}_s, \mathbf{q}_i) \neq \phi(\mathbf{q}_s)\phi(\mathbf{q}_i)$, that is, an entangled two-photon state.

The modulus of the mode function now describes the photon-pair detection probability in a far field imaging system, that is, in the Fourier plane of a $2-f$ imaging system. For quantum imaging approaches that exploit the spatial correlations, it is desirable to have a large bandwidth of involved \mathbf{q} -vectors as well as near-perfect correlations to obtain the best possible resolution. These requirements are met in the limit of a wide and short nonlinear crystal $L \rightarrow 0$ using a plane wave pump mode ($w_p \rightarrow \infty$), where the transverse wave vectors become perfectly anticorrelated^[44]

$$\phi(\mathbf{q}_s, \mathbf{q}_i) \approx \delta(\mathbf{q}_s + \mathbf{q}_i) \quad (6)$$

This is intuitively clear as a consequence of momentum conservation in the transverse plane. Likewise, by Fourier transform of this expression we find that the photons also emerge from the exact same point in the crystal plane

$$\phi(\mathbf{r}_s, \mathbf{r}_i) \approx \delta(\mathbf{r}_s - \mathbf{r}_i) \quad (7)$$

These perfect (anti-)correlations of emission points in the near field and transverse momentum (i.e., emission angles) in the field are an embodiment of quantum entanglement.^[44,46,55] Achieving such perfect correlations by limiting the SPDC interaction to very short materials with a large aperture, while at the same time achieving the conversion efficiency required for practical applications, is the subject of ongoing research (see also Section 6).

We should also point out, that Equation (4) expresses the biphoton state in terms of a transverse plane wave decomposi-

tion, which is convenient when we are interested in the far field distribution of the emission detection modes. In particular, in coherent quantum imaging schemes, it can be more useful to express the biphoton state in terms of other modes, for example, by decomposition into Laguerre–Gauss modes with a radial mode index p and the topological winding number l as

$$|l, p\rangle \equiv \int d\mathbf{q} U_{lp}(\mathbf{q})|\mathbf{q}\rangle \quad (8)$$

In this basis, we can decompose the biphoton mode function as [48]

$$|\Psi\rangle = \sum_{p_1, p_2}^{l_1, l_2} C_{p_1, p_2}^{l_1, l_2} |l_1, p_1\rangle_s |l_2, p_2\rangle_i \quad (9)$$

where l_1, p_1 denote the mode indices of signal and p_2, l_2 those of the idler, respectively. The mode amplitudes $C_{p_1 p_2}^{l_1 l_2}$ are calculated by projecting the biphoton state in free space (Equation (5)) onto the respective target modes

$$C_{p_1 p_2}^{l_1 l_2} = \int d\mathbf{q}_s d\mathbf{q}_i \Phi(\mathbf{q}_s, \mathbf{q}_i) U_{l_1 p_1}^*(\mathbf{q}_s) U_{l_2 p_2}^*(\mathbf{q}_i) \quad (10)$$

In the concrete example of Laguerre–Gauss modes, the signal and idler photons carry a well-defined orbital angular momentum (OAM) of $l\hbar$. Since for a Gaussian pump beam $l_p = 0$ and OAM is conserved in the collinear SPDC process, we have $l_p = l_1 + l_2 = 0$, that is, OAM entanglement. The exploitation of OAM beams, and other discrete mode decompositions (e.g., Hermite–Gauss modes) has been proposed for applications in enhanced phase contrast microscopy.^[56,57] Exploring similar techniques at the single-photon level while exploiting the spatial correlations of OAM-entangled states thus seems promising.

The description in terms of a modal distribution is also relevant in experimental scenarios, where photons are required to be coupled into single mode fibers. The probability of collecting a photon pair per Hz bandwidth per pump photon (spectral brightness) into the fundamental mode of a pair of single-mode fibers is then given by $|C_{00}^{00}|^2$. To maximize the fiber coupling efficiency, a focused pump beam and a longer nonlinear crystal are required. In fact, it has been shown that strong pump focusing, which minimizes the amount of spatial entanglement, is required to maximize the fiber coupling efficiency.^[58] Using strongly focused pump beams, pair detection rates in excess of 1 million pairs per mW of pump power have already been demonstrated.^[59] Further improvement of the pair collection efficiency of photons pairs, while also ensuring spectral purity and other desirable features such as polarization-entanglement, is the subject of a vast amount of ongoing research.^[29,41,60]

3. Interference-Based Quantum Imaging

In the beginning of the twentieth century, when the foundations of quantum physics were developed, one of the most fascinating phenomena was the wave-particle duality of quanta, such as photons. Several double slit experiments have been envisioned and performed to investigate and illustrate this intriguing behavior.

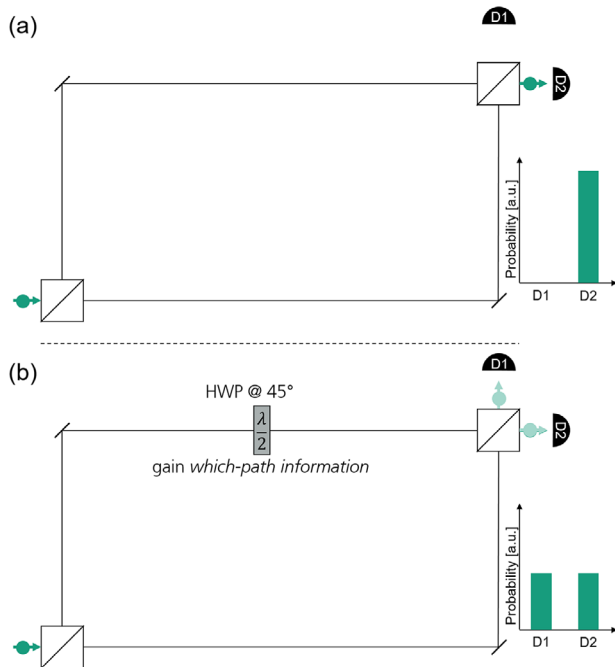


Figure 3. Which-path information in a Mach–Zehnder interferometer. a) Single photons (and coherent laser) light will behave as a wave and coherently propagate through the interferometer, since both path possibilities are indistinguishable. b) Marking one of the paths, for example, by changing the polarization in there with a half-wave plate (HWP); thus, gaining which-path information destroys the coherent behavior and the photons act as classical particles.

As it turned out, the wave or particle nature of photons is always linked to the possibility (or impossibility) of distinguishing the paths they took. This very principle of quantum mechanics can be applied for novel imaging and spectroscopy approaches.

3.1. Induced Coherence and Nonlinear Interferometers

To explain wave-particle duality and the distinguishability of path possibilities, we first discuss the Mach–Zehnder interferometer (MZI) with exactly equal arm lengths as sketched in **Figure 3**. Its behavior is well known for classical laser light, which is coherently split at the first beam splitter and due to interference, which is associated to the wave nature of light, in a second beam splitter it emerges only from one output port. Replacing now the laser light by a stream of single photons will yield exactly the same outcome. Photons will only be detected in one of the output ports of the second beam splitter as sketched in **Figure 3a**. This happens only due to the absence of *which-path information*, that is, the knowledge of which particular path a particular photon propagated through the interferometer. Hence, the interference effect should disappear whenever one gains which-path information. By making the paths distinguishable, for example, by changing the polarization of the photons traveling through it as shown in **Figure 3b**, the photons start to behave as individual particles instead of interfering waves. Accordingly, photons will be present in both output ports of the second beam split-

ter (see **Figure 3b**). In this regard, one could state that by erasing which-path information, coherence or coherent behavior is induced.

In 1991, Mandel and co-workers applied this very principle to non-linear interferometers where they found such induced coherence^[61,62] in SPDC. In their work, two nonlinear crystals were coherently pumped by splitting the pump at a beam splitter (see **Figure 4**). The idler photons from the first crystal were aligned with the idler photons from the second one in order to make the two path possibilities indistinguishable. This way coherence is induced between the signal photons from the two downconversion processes and they interfere if they are overlapped using a beam splitter. This is visible by the interference fringes in the single counts in one of the output ports of the beam splitter when moving it stepwise. However, the interference between the signal photons is erased when the idler beam from the first crystal is blocked before entering the second crystal. In that situation, one could in principle distinguish if an idler photon was generated in the first or the second crystal by placing a detector in the idler arm and correlating its measurements with the signal detector. Both detectors would click simultaneously when a the photon pair was generated in the second crystal, whereas only the signal detector would measure a photon when the pair originated from the first crystal. This means, that both possible paths of the signal and the idler photons become distinguishable. This distinguishability removes the coherence between the signal photons generated in the two crystals, even if no idler detector is present. Consequently, the interference vanishes from the detected single counts of the signal upon movement of the beam splitter. It was also demonstrated that when introducing an object between the two crystals, the degree of coherence varies with the transmittivity of that object. That results in a change of the visibility of the interference fringes, canceling out the interference when the transmittivity equals zero as we just described, and being maximum when the transmittivity equals one. This way, information about the object can be obtained as it will be further discussed in the next Section 3.2.

It is important to emphasize several points here: i) no coincidence detection is involved in order to observe this effect of induced coherence, ii) the signal photons showing changing visibility of interference never interacted with the object, and iii) there is no induced emission in the second nonlinear crystal due to the idler beam from the first crystal, that is, the effect results from interference of the probabilities of creating a photon pair either in the first or the second crystal.^[63]

3.2. Quantum Imaging with Undetected Photons

In the previous section, the concept of induced coherence in a nonlinear (Mandel) interferometer was introduced. This concept can be applied for spectroscopy (see Section 3.3) and quantum imaging with undetected photons, as demonstrated by Lemos and co-workers.^[5] In this imaging method, the photons illuminating the sample are not detected at all and the photons that are detected never interacted with the sample. This scheme is highly interesting since it brings new flexibility to the spectral ranges at which the properties of objects can be measured. The wavelength

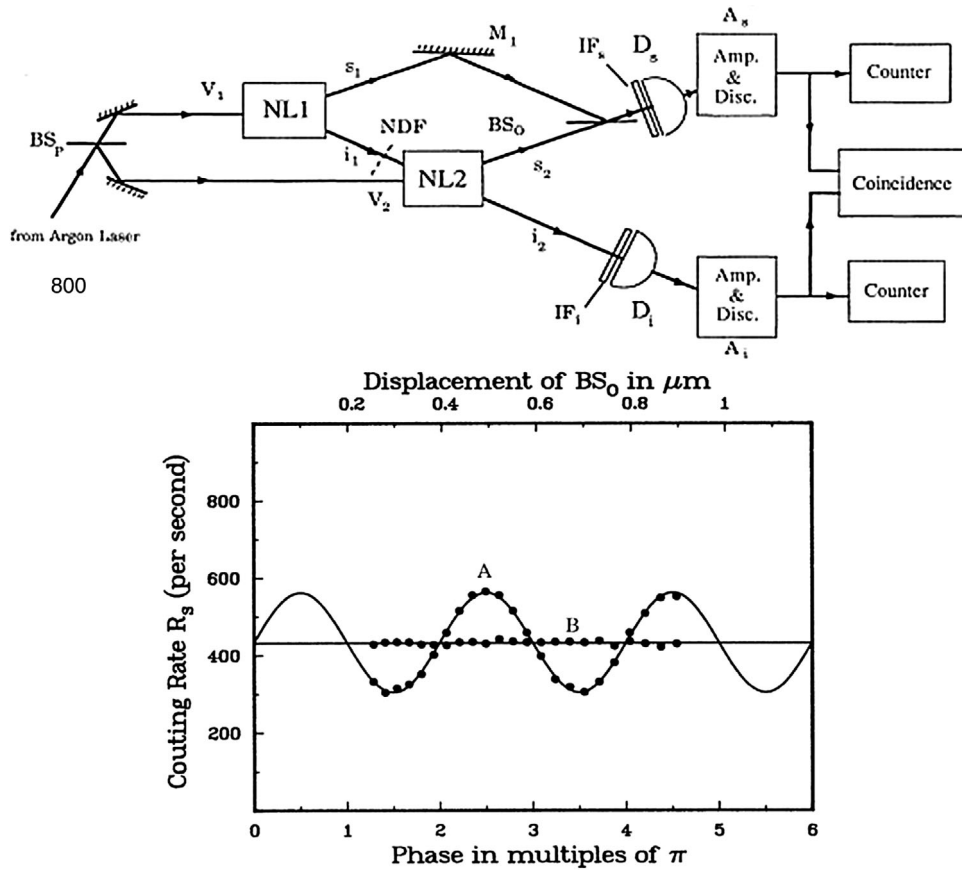


Figure 4. Induced coherence without induced emission. Top: Experimental setup based on two nonlinear crystals (NL1,2), which are coherently pumped. If both idler beams are overlapped to be indistinguishable, the corresponding signal beams show interference at a beam splitter (BS_0). On the contrary, gaining which-path information lets the signal interference vanish. Bottom: Experimental results obtained with the setup above. Curve A shows the photon counting rate R_s obtained from detector D_s when placing a filter (NDF) with high transmission 0.91 between NL1 and NL2. It shows interference behavior. Curve B shows the count rate when the beam between the two crystals is blocked. In this case, the source of the photons at the beam splitter is known and there is no interference pattern. Reproduced with permission.^[61] Copyright 1991, American Physical Society.

of the illuminating photons is now not limited by the availability of suitable detectors.

The setup for the first imaging demonstration is based on the one used by Mandel for demonstrating the induced coherence phenomenon. It is depicted in **Figure 5**. Additional lenses implement the imaging system, where the plane of the first nonlinear crystal (NL1) is imaged onto the plane of the second nonlinear crystal (NL2) with the object in the Fourier plane.^[64,65] The object plane itself is imaged onto the electron multiplying charge-coupled device (EMCCD) camera. Due to the indistinguishability between the possibilities were a detected idler photon was created in the first nonlinear crystal, and thus passed through the object before detection or were it was created in the second nonlinear crystal, and thus did not interact with the object at all, the object can be observed as interference image in the signal beams after passing a beam splitter (see **Figure 5**).

In detail, assume that the object between the two crystals has a real transmittance $T(x, y)$, which depends on the spatial coordinates x and y , and also causes a phase shift $\gamma(x, y)$ to the idler photon that passes through the object. Then, a straight forward analysis shows that the probability of detecting signal photons in the beam splitter output ports denoted by L5 and L6 in

Figure 5 is

$$P_{L5/L6}(x, y) = \frac{1}{2}[1 \pm T(x, y) \cos \gamma(x, y)] \quad (11)$$

It follows, that two kinds of imaging can be observed: one based on constructive and one based on destructive interference realized by the different signs in Equation (11). As discussed earlier, the transmittance of the object determines the which-path information, and thus, the visibility of the interference fringes. In the extreme case, when $T = 0$ (idler beam path is blocked), the interference completely disappears and no image can be observed. Additionally, the phase introduced by the object creates a different path length of the photons that can be observed by the two emerging interference pictures as well. The phase difference is determined by the path length difference of the light actually going through the object rather than the light detected by the camera. Interestingly, as Lemos and co-workers demonstrated, objects that are not even transparent to the light that is used for imaging on the camera can be observed by illuminating them with light, which is not detected and to which the camera not even needs to be sensitive.

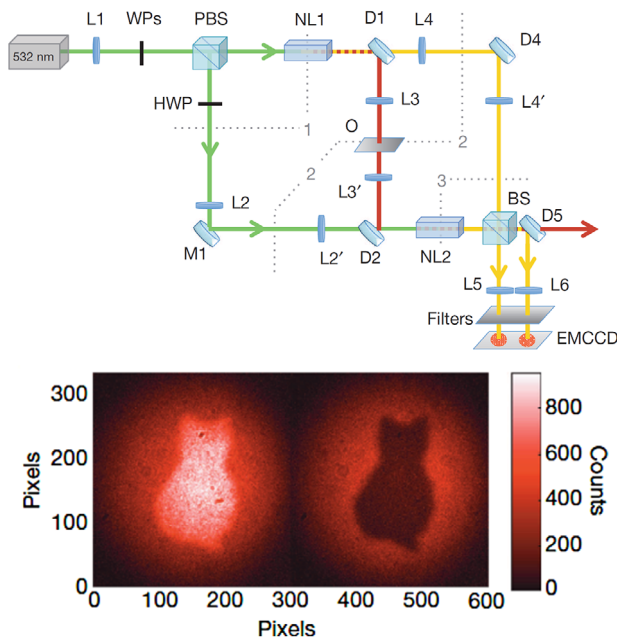


Figure 5. Experimental setup for imaging with undetected photons (top). Intensity image (bottom): constructive and destructive interference images taken at the outputs of the beamsplitter (BS) when placing the object O between dichroic mirrors D1 and D2. Reproduced with permission.^[5] Copyright 2014, Springer Nature.

As previously mentioned, this interference-based imaging configuration offers interesting applications since non-degenerate SPDC allows the generation of photon pairs with extreme wavelength difference. This way, photons in the VIS range and their partners in the deep UV or THz range can be harnessed. Si-based VIS detection is highly efficient, reliable and economic. Since this does not apply for UV or THz detection, quantum imaging via a nonlinear (Mandel) interferometer can be used to overcome this issue. In particular, for the UV range one can find applications beyond physics, for instance in biology, metrology, and lab-on-chip lithography. These applications would not only benefit from the enhanced detection efficiency of the VIS detectors but also from the minimum photon dose to not damage biological samples or to be classified as eye-safe technology.

However, current setups based on induced coherence are purely academic so far. To be applicable, for example, inside a life science laboratory, the SNR needs to be maximized^[66] and system integration is necessary. A more compact and stable configuration is possible by utilizing one crystal only, which is pumped by the same laser from two sides.^[67] Single frequency pumping is beneficial in any case to guarantee a high degree of correlation between the generated signal and idler pairs. Moreover, harnessing only a single crystal additionally circumvents the issue of reduced contrast caused by partial distinguishability of the two crystals. This could be an essential step for an actual device development for this kind of quantum imaging.

We would like to mention a possible extension of this scheme by employing multiphoton events. The general SPDC state is known as two-mode squeezed vacuum and includes higher-order pair emission.^[68,69] Applying a SPDC process

with sufficient strong pump (but still within the spontaneous regime) or with a pulsed pump to have non-negligible higher-order pair events—most likely pairs of pairs—will lead to have single photons as well as pairs in the signal and idler beams, respectively. In addition, the usage of photon number resolving detectors (see Section 6.2) allows to select measurement events only caused by pairs (in the signal beam, so no coincidence measurements). The advantage of such photon pair states in signal and idler beam is the same as for N00N state microscopy (see Section 5.2). Both approaches are based on the interference of N photons going one or another way. An object with phase function $\gamma(x, y)$ in one of the arms causes a phase shift of $N \times \gamma(x, y)$ for this particular path possibility. Hence, one can achieve an enhanced phase sensitivity and accuracy below the shot noise limit. As difference, in the quantum imaging scheme based on induced coherence the actual detection is performed with the corresponding partner photon pair. Despite the fact that most likely $N = 2$ it can already enhance the sensitivity of the quantum imaging scheme with undetected photons.

Recently it was also reported how methods of classical optical coherence tomography may be translated to new wavelength regimes using the effect of induced coherence. In ref. [70], Valles et al. used induced coherence in conjunction with frequency-entangled photons to achieve axial sectioning of a partially reflective specimen. The approach is particularly intriguing for sectioning bio specimens, where it could enable deeper penetration into samples due to longer wavelength probe photons.

3.3. Quantum Spectroscopy

As it was previously introduced, photons generated in SPDC processes are entangled in frequency since energy conservation has to be fulfilled during the process (see Equation (2)) and the signal and idler wavelengths can be very different. Hence, adopting the induced coherence approach as discussed previously, quantum spectroscopy in technically hardly accessible spectral ranges with detectors for the visible (VIS) spectral range becomes possible, leading to higher quantum efficiencies, lower noise levels, and reduced cost.

This spectroscopy approach is most interesting in the Mid-IR to THz spectral range, where many molecules have their spectroscopic fingerprints. Albeit light sources are available for such wavelengths, detectors to cover the Mid-IR to THz regime suffer from noise, are expensive, or do not even exist.

A first experimental realization of SPDC-based spectroscopy was demonstrated by Kalashnikov and co-workers in 2016,^[6] a sketch of their experiment is shown in **Figure 6a**. To realize their nonlinear interferometer, they employ two nonlinear crystals for SPDC in a row, which both are pumped by the same laser beam. They generate photon pairs with signal photons in the VIS spectral range and idler photons in the Mid-IR. The analyzed gas is between the two nonlinear crystals, so that both signal and idler generated in the first crystal are transmitted through the gas before interfering with the signal and idler photons in the second crystal. However, the gas needs to be completely transparent for both the signal and pump wavelengths. In this case, as described before, the transmittance of the gas for the idler

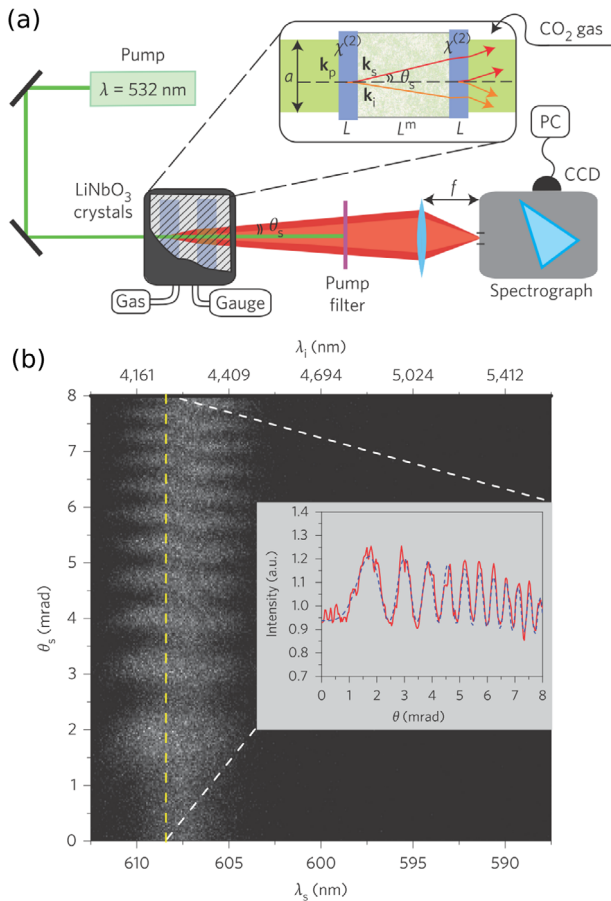


Figure 6. a) Quantum spectroscopy experimental setup presented by Kalashnikov et al.^[6] b) Measured 2D interferogram with a single spectral component plotted in the inset. a, b) Reproduced with permission.^[6] Copyright 2016, Springer Nature.

wavelength influences the visibility of interferences between signal photons generated in both nonlinear crystals. For the measurement, an imaging spectrometer is employed. An example for a measured 2D interferogram, measured in the VIS spectral range, is depicted in Figure 6b, where also the corresponding idler wavelengths in the Mid-IR are indicated. The fringes in the vertical direction stem from interference of different spatial modes emitted by both crystals under different angles. A theoretical fit of this interference pattern yields both transmission and phase shift due to the medium under test. Hence, this nonlinear interferometer can be applied to simultaneously measure the refractive index and absorption of a medium in the Mid-IR range with VIS equipment. This technique provides a direct measurement, does not suffer from losses because of water vapor absorption and has an accuracy of (5×10^{-6}) in determination of CO₂ refractive index comparable with state-of-the-art IR methods. Recently, a similar experiment has been demonstrated that avoided using a monochromator by directly imaging the diffraction pattern on a camera and using a single SPDC source with narrow emission spectrum^[71] which was pumped from both sides. For changing the wavelength, the phasematching condition of the SPDC crystals was changed by rotating the crystal. Due to a more

efficient use of the generated photons, this method provides an improved SNR. The spectral resolution of the system is now limited by the SPDC linewidth instead of the spectrometer, meaning that it can be controlled by the length of the used crystals.

Fully integrated spectroscopy based on SPDC can in principle also be realized, as has recently been conceptually suggested in a lithium niobate waveguide.^[72] Integration in waveguides, where the interaction with the medium under test can be achieved via evanescent fields or coupling to adjacent liquid channels, would provide ultimate stability and miniaturization.

4. Correlation-Based Quantum Imaging

The imaging and spectroscopy schemes discussed up to now were based on detection of only one photon of the pair generated by SPDC, where the second photon is used to mediate the interference between the different possible origins of photon pairs. Imaging schemes in which still only one photon interacts with the sample but both are detected will be the topic of this section. Here, the formation of the measured image is due to the spatial correlation between the two photons of a pair.

4.1. Quantum Ghost Imaging

The best known among such imaging schemes is the quantum ghost imaging (QGI), principle of which is schematically depicted in Figure 7a. Here, the two photons of a correlated photon pair generated by SPDC are split into two separate beams. One of these beams, for example, the signal, is used to illuminate the object, the transmitted signal photons are subsequently detected using a so-called bucket detector. The idler beam, on the other hand, is characterized by a spatially resolving single-photon detector, which can be either implemented using an array detector or a single scanning detector. Both detectors on their own cannot generate an image of the object, as one of them does not receive any spatial information, the other does not receive information about the object. However, the image appears in the correlation signal of the two measurements. This imaging scheme uses the fact that the photons of a pair appear always perfectly correlated in time and ideally also in space, as discussed in Section 2. Thus, the measurement of the position of the idler photon with the spatially resolving detector is sufficient to determine the position of the signal photon on the object, while measuring the transmitted photons statistics eventually will lead to an estimate of the object transmission at that position.

Many properties of this simple scheme can be more intuitively understood using the Klyshko picture,^[73] where the nonlinear crystal that generates the photons is thought of as a linear mirror that reflects photons originating from a point source at the position of the bucket detector toward the camera, as shown in Figure 7b. In the unfolded version of this scheme, the upper arm in the sketch is folded around the plane of the nonlinear crystal/mirror, which then acts simply as an additional aperture.

Ghost imaging (GI) can be also realized with thermal light or coherent light modulated spatially in a suitable way. Here, the fluctuating beam is split using a beam splitter and the sample is

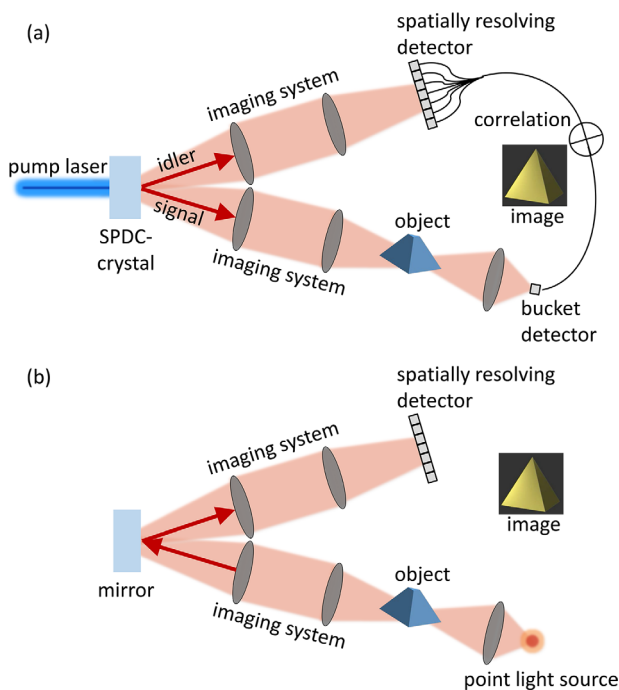


Figure 7. a) Sketch of quantum ghost imaging. Photon pairs are generated by spontaneous parametric downconversion (SPDC) in a nonlinear optical crystal pumped by a laser; the signal and idler photons are subsequently separated. The idler photons are imaged onto a spatially resolving single-photon detector without interacting with an object. The signal photons are imaged onto the object and, after transmission, collected with a bucket detector. The image can be obtained by correlating the measurements of both detectors. b) Klyshko representation of the imaging scheme depicted in (a), where the bucket detector and the nonlinear crystal are replaced by a point light source and a mirror, respectively. This representation can serve as an intuitive guide in determining the properties of quantum ghost imaging.

again placed in one arm with a bucket detector, whereas spatially resolved detection takes place in the second arm of the measurement device.^[74,75] In a sense, using correlated photon pairs is just a specific way to implement the spatial modulation needed to establish spatial correlation between the two measurement arms. In principle, each GI scheme that can be implemented with photon pairs may thus be realized also with classical light. However, due to the fundamentally different statistical properties of coherent and thermal light on one side and photon pairs, that is, number states, on the other side, differences in the SNR of the obtained images appear^[76] which point to a fundamental advantage in using photon pairs in this respect. Here, we will concentrate on the works that discuss QGI with photon pairs.

The first detection scheme of this type was realized using only diffraction and hence was dubbed ghost diffraction (GD).^[77] Here, no imaging optics was used as shown in the sketch of the experiment in **Figure 8**, the object was simply placed in one of the separated photon beams, while the bucket detector D1 was placed behind a small aperture, thus measuring only photons in a specific spatial mode. This aperture is crucial for the formation of the diffraction pattern in the measured coincidences, as collection of multiple modes leads to immediate blurring of the measured diffraction pattern.^[78] Essentially, as can be understood using the

Klyshko picture, this effect corresponds to classical diffraction, where one coherent mode is needed for illumination of the object in order to generate a diffraction pattern. Widening the aperture in GD would correspond to using a spatially extended incoherent light source in the classical representation, thus washing out the interference. The GD method was also applied to measure phase-only objects,^[79] as they also produce a notable diffraction pattern.

QGI was first implemented in 1995^[80] by adding just one imaging lens to the original GD setup. The placement of the lens is ruled by a modified Gaussian lens equation. In the Klyshko representation of the experiment, this lens needs to be placed in a way to image the object onto the detector.

The experiments described up to now obtained spatial resolution by scanning a single photon detector across the positions to be measured and collecting correlation counts for a fixed time at each point. Experiments involving arrayed detectors were performed only after intensified CCD (iCCD) cameras became available, which provided sufficient detection efficiency of a few ten percent and temporal discrimination to perform correlation measurements. The latter was achieved by triggering the image intensifier with the detection signal from the bucket detector, images were obtained by integrating many intensifier frames in one CCD readout.^[81–83]

A related approach was realized by imaging both the signal beam transmitted through the object and the idler beam on two separated areas of the same CCD-sensor^[10,84,85] as shown in **Figure 9**. Here, instead of sequentially measuring each photon pair, the camera records both the spatial distribution of the signal photons that passed through the sample and the spatial distribution of the idler photons. The latter can be used to normalize the measured transmission image, thus obtaining a faithful image of the object.

It could be experimentally shown that this imaging scheme, implemented with high-efficiency EMCCD cameras, can surpass the classical noise limit and can perform subshot noise imaging.^[10,84,85] This capability is due to the perfect correlation between signal and idler photons, which ensures that they share exactly the same statistics. This advantage is in principle also possible in QGI using single-photon correlation measurements, which has been discussed theoretically already very early.^[86,87] However, experimentally it was up to now only realized in spectroscopy experiments with only one spatial mode.^[88,89] It was also shown experimentally, that this advantage is only possible in QGI and cannot be realized in similar ghost imaging schemes with classical light sources.^[74,90] The advantage of QGI with respect to classical GI is largest for small illumination levels,^[76] where the classical Poissonian statistics yields a large relative uncertainty, and for high detection efficiency and low absorption in the sample, that do not introduce Poissonian uncertainty outweighing this advantage. Thus, QGI seems to be especially suitable for imaging objects that are very sensitive to illumination, as it can extract a maximum of information from each photon passing the object. This may be especially valuable for short wavelengths, where samples under test can easily be modified or damaged by light. Furthermore, it can be used to detect objects in the presence of background light of similar or larger intensity than the quantum light beam used to probe the object.^[85,91–93] As was shown recently, the needed illumination level for reaching a certain SNR can be further reduced when placing the object in one

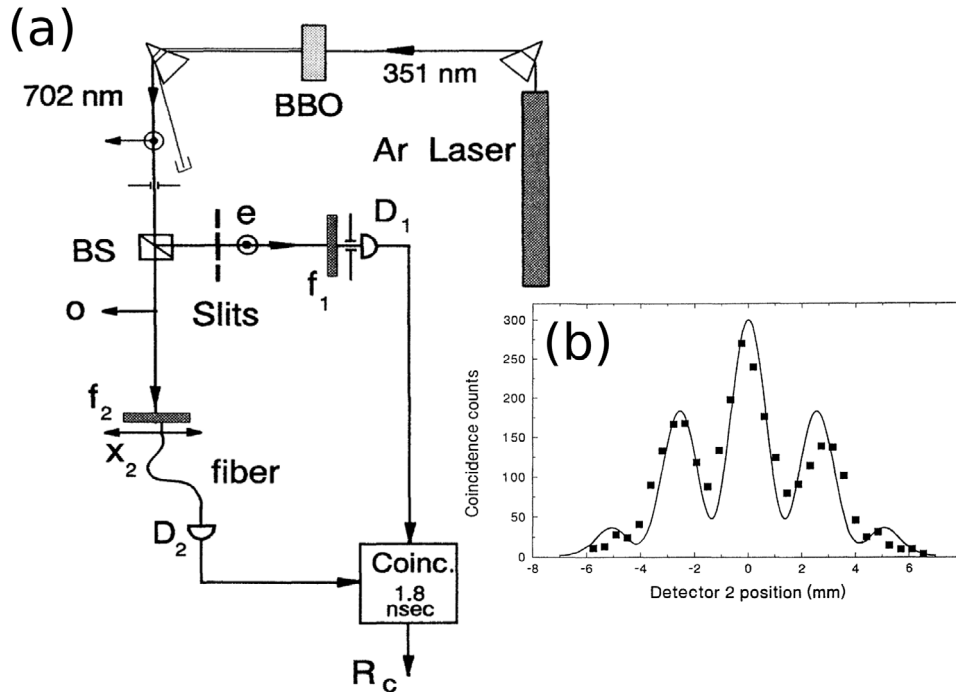


Figure 8. a) Sketch of the experimental setup for the implementation of ghost diffraction. b) Measured diffraction pattern obtained by correlating the single-photon counts detected by the fixed detector D_1 , which is placed behind an aperture and detects signal photons transmitted by the sample, and the moving detector D_2 , which detects the idler photons. a,b) Reproduced with permission.^[77] Copyright 1995, American Physical Society.

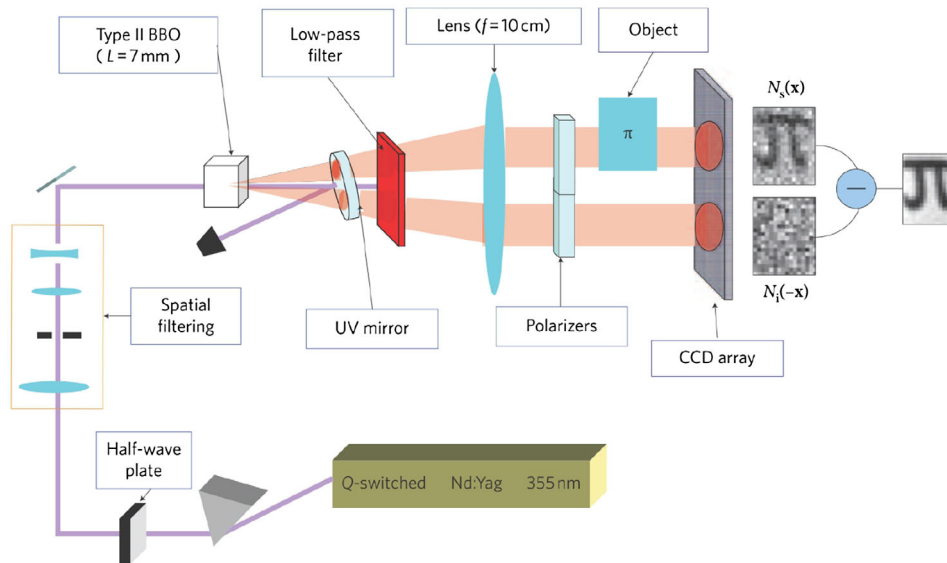


Figure 9. Scheme of subshot noise imaging, where signal and idler photons are separated into two beams, one of which is transmitted through the object, and both of which are detected by a CCD camera. Reproduced with permission.^[84] Copyright 2010, Springer Nature.

arm of a linear interferometer, which is passed by only the signal photons.^[94] The object disturbs the interference, leading to a measurable signal. The lower number of photons needed to interact with the object is due to the fact that also photons passing the interferometer in the arm without the object will contribute to the measured information.

Using two paired photons to measure an image also entails the possibility that they can have different wavelengths, which in

general can be easily achieved in photon-pair generation using SPDC. QGI with two different wavelengths has been demonstrated theoretically and experimentally,^[4,95–97] showing that the sample under test can be imaged in wavelength ranges for which no imaging detector is available. For instance, in ref. [97], photon pairs with one photon in the visible spectral range and one photon in the near-infrared (NIR) at 1.5 μm wavelength were used. The NIR photon was impinging on a sample and measured with

a single bucket detector, whereas the visible photon was characterized by a camera without interacting with the sample. The measured image was determined by the sample properties in the NIR. In contrast to imaging with undetected photons as described before, in QGI for each used wavelength at least a single bucket detector needs to be available. On the other hand, the advantage in terms of the achievable SNR becomes available only in this case.

An intriguing question is that for the spatial resolution achievable in QGI, especially in the case of non-degenerate photon pairs. Early demonstrations of QGI with degenerate photon pairs seemed to demonstrate an enhanced resolution with respect to classical imaging using the wavelength of the photon pairs.^[98] However, theoretical works concluded, that the resolution cannot be better than the one given by the wavelength of the photon pair, and is usually worse due to finite-sized pump beams and crystal lengths,^[99,100] which was recently shown also experimentally.^[101] This can be intuitively understood in the Klyshko representation, where the pumped nonlinear crystal is just another aperture, which can influence the resolution only by degrading it. The same result was obtained for QGI with non-degenerate photon pairs,^[3,95] although a higher field of view without degradation of the resolution was shown.^[4,102] However, for ghost diffraction, it was predicted that for strongly non-degenerate photon pairs, diffraction from periodic structures can be measured, which period is much below the wavelength of the idler photons that are detected by the spatially resolving detector.^[103]

4.2. Quantum Ghost Spectroscopy

The basic principle of ghost imaging, namely using two correlated beams of light to perform measurements, can be extended to obtain different properties than the spatial distribution of a 2D object, which in QGI becomes possible due to the correlation in the “birthplace” of signal and idler photons of a pair. In addition, also the spectral properties can be determined using quantum ghost spectroscopy (QGS). Here, the fact is used that due to energy conservation the frequencies of signal and idler photons are strictly anticorrelated, as the sum of signal and idler photon energies has to be equal to the energy of a pump photon.

This was first implemented using degenerate photon pairs in the visible spectral range.^[104–106] In these experiments, spectrally broadband photon pairs were generated into a single spatial mode and separated into signal and idler beams. The sample was placed in one beam, the transmitted photons were measured using a single detector. Spectral resolution was obtained by filtering the second beam with a tunable monochromator in front of the second detector, whose measurements were correlated with the measurements of the first detector. The number of the coincidences as a function of the frequency selected by the monochromator is proportional to the transmission of the sample at the frequency of the idler photon, $R(\omega_s) \approx T(\omega_i = \omega_p - \omega_s)$. This way, by scanning the spectral range of the signal arm with the monochromator, the spectral properties of the sample can be analyzed. Again, two different spectral ranges could be used for signal and idler,^[107,108] hence, with a monochromator and detector

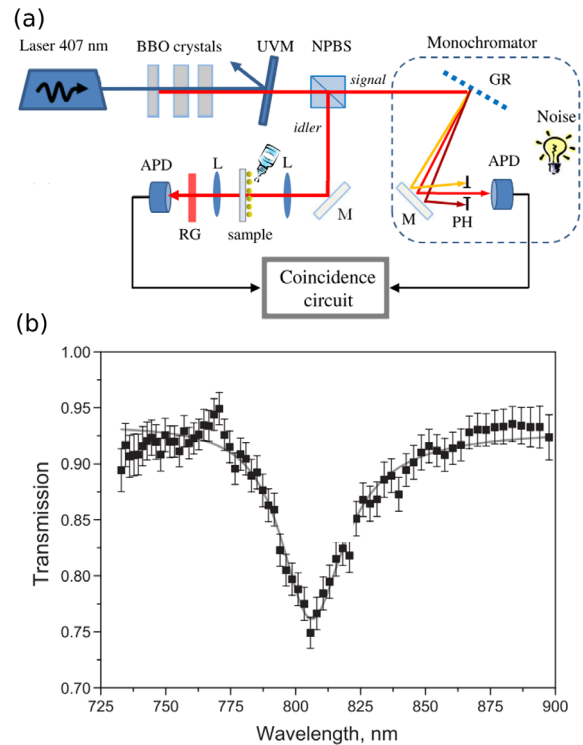


Figure 10. Sketch of the setup for quantum ghost spectroscopy. Photon pairs with large spectral bandwidths are generated by three cascaded BBO crystals. The signal photons are analyzed with a single-photon-sensitive spectrometer; the idler photons transmit through the object and are detected by a single-photon detector without spectral resolution. The spectrum can only be obtained by correlating the measurements of both detectors. b) Measured spectrum of plasmonic nanoparticles with a resonance round 800 nm. a,b) Reproduced under the terms of the CC-BY Creative Commons Attribution 3.0 License. (<https://creativecommons.org/licenses/by/3.0/>).^[109] Copyright 2014, The Authors, published by American Physical Society.

optimized for one spectral range, a wide range of spectroscopic applications can be addressed.

One advantage of using correlated photon pairs, namely the increased signal-to-noise level, has been used extensively in QGS. Using correlations also enables measurements that are more robust against external noise which may be present in the measurement system due to, for example, stray light, as this will not lead to correlation counts. Kalashnikov and co-workers in 2014^[109] successfully showed QGS under very noisy conditions, while a comparable conventional spectroscopy approach failed (see **Figure 10**). The ratio of the SNR for conventional spectroscopy and QGS is

$$\frac{SNR_Q}{SNR_T} = \frac{\eta_i}{N_i \Delta t} \quad (12)$$

where SNR_T and SNR_Q are the conventional and QGS SNR, respectively. η_i is the detection efficiency for the idler channel, N_i is the number of noise photocounts of the idler arm APD and Δt is the coincidence window of the coincidence circuit. As Equation (12) shows, the SNR_Q advantage is improving with

high detection efficiency, low-noise detectors in the idler path, and narrow coincidence time windows.

4.3. Applications and Challenges

As discussed before, the fundamental advantage of QGI and QGS is that the SNR of a measurement can be better than achievable with classical light. This can be used in two different application cases. First, it allows to measure with comparable SNR to classical techniques while using a lower amount of photons. This is relevant for objects that are sensitive to light, for example, in the biological and life sciences. It can be especially useful when measuring at short wavelengths, especially in the UV spectral range and below, where classical GI was already demonstrated for X-rays.^[110,111] The number of needed photons may be further reduced by using techniques as compressed sensing,^[82,112] which faithfully reconstruct images from an incomplete amount of measured information. In the second application, the better SNR of QGI and QGS is used to enhance measurements in environments inducing noise, for example, due to scattering.^[113] Using such measurement approach could improve imaging over long distances through moving atmospheres or fog as well as imaging through tissue.

Furthermore, QGI offers other practical advantages that stem from the fact that the two photons could be used for independent measurements, although only one interacts with the sample. This means, in principle two different types of information can be obtained simultaneously, thus maximizing the gained amount of information from the available photons. For instance, the bucket detector in QGI could be replaced by a spectrally resolving detector array, which would enable to obtain multispectral ghost images, thus combining the discussed techniques of QGI and QSI. Another approach is the so-called plenoptic GI, in which the single detector of conventional GI is replaced by another spatially resolving detector that monitors the spatial spectrum of the signal photons passing the object.^[114,115] Thus, the 3D geometry of an object can be obtained. This scheme has been experimentally demonstrated with a classical light source^[116] and holds promise for the realization of low-illumination-power 3D imaging. These approaches offer the advantage that, if suitable detectors are available, they simultaneously can achieve a high resolution in both the spatial and the spectral/spatiospectral domain without sacrificing photons by filtering or enlarging the needed bandwidth. For example, in classical multispectral imaging, either a narrow spectral filter is employed for each wavelength channel, thus absorbing the other spectral components, or a large number of images are taken simultaneously, necessitating a large number of detectors. In QGI, two detectors measuring in the needed domains are sufficient and no filtering is needed.

In addition to measuring two different types of information simultaneously, the correlations in different degrees of freedom present in photon pairs can be also used together, for example, to transmit images through single-mode fibers.^[117] In this experiment, broadband idler photons were dispersed spatially in a way, that each position on the object was illuminated with a different spectral component. After reflection from the object, all spectral components were coupled to a single mode fiber and transmitted to the bucket detector. Due to dispersion the differ-

ent spectral components had different arrival times, which could then be mapped onto the spatial positions on the object using correlation measurements with a single detector measuring the signal photons.

Although the discussed approaches for QGI and QGS have fundamental advantages over classical measurement techniques and could be envisioned in a number of applications, several technological challenges remain before a full assessment of the applicability can be made. These challenges are to experimentally realize the fundamental advantage of better SNR and doing so in a way that is suitable for applications. To realize the increased SNR, the main necessity are detectors with quantum efficiencies close to unity in the needed spectral regions and the ability for a very fast gating. Whereas for the visible and near-infrared fast single-photon detectors with efficiencies close to 0.9 are available, for other spectral regions of interest the efficiencies are much lower. Even more development is needed for suitable cameras, although they ideally have to detect only in the visible spectral region. Here, there currently is no solution which combines high quantum efficiency and fast gating.

To apply QGI and QSI, also sources in the addressed spectral ranges are needed, which should provide a large number of spatial or spectral modes to enable a high resolution in the respective domain. Furthermore, measurement times have to be reduced from the now needed minutes or even hours to obtain one image down to the second range. To achieve this, the sources have to be optimized for generating more photon pairs. Additionally, detection as well as correlation electronics must be fast enough to handle correlation rates of several MHz.

Finally, cameras not only enabling fast gating but being able to perform photon timing are needed to rid optical setups for QGI from the up-to-now needed imaging delay lines. Only then, compact measurement devices reminiscent of conventional microscopes but employing QGI seem feasible. Subshot noise imaging, where both photons are measured using conventional CCD sensors, was already implemented in a microscope.^[10]

5. Entanglement-Based Quantum Imaging

As seen in the previous sections, already the interaction of one photon of a photon pair with the sample can lead to intriguing physics and sophisticated applications. However, entanglement, probably the most unique feature of quantum mechanics, is in general not used. It can only be harnessed when both photons of the used pairs interact with an object.^[118] The advantage of using entanglement can be further enhanced when using non-classical states of more than two photons. One interesting class of states with two or more photons are the so-called N00N states,^[119] N -partite entangled states where one mode is occupied by N photons, whereas the other is in vacuum or vice versa. Those states will play a central role in the second part of this section, whereas we focus on a multiphoton microscopy approach at the beginning.

5.1. Photon Pair Fluorescence Microscopy

Fluorescence microscopy is one of the major tools in the area of life science. Harnessing autofluorescence of several

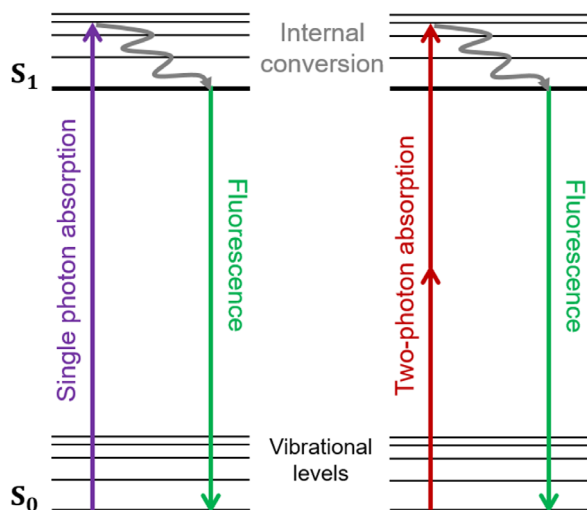


Figure 11. Jablonski energy diagram. A single photon with sufficient energy can be absorbed and by a molecule and excites it from the electronic ground state S_0 to the first excited electronic ground state S_1 . After an internal conversion (non-radiative decay) toward the vibrational ground level within S_1 a fluorescence photon is emitted at lower energy. The same process can be driven by absorbing two photons simultaneously with sufficient energy in sum.

molecules or labeling functional cell parts with fluorophores allowed completely new perspectives in bio-medical research and diagnostics.^[120,121] Extending it to confocal laser scanning microscopy enabled significantly enhanced image quality in terms of axial resolution and reduction of out of focus light.^[122] **Figure 11** sketches the energy (Jablonski) diagram of the fluorescence process. Light with sufficient energy excites a molecule from the electronic ground state to the first excited electronic state. After relaxation to the vibrational ground level within the excited electronic state, fluorescence emission at longer wavelength than the excitation is observed with a typical lifetime in the range of nanoseconds. The excitation can also be realized by a multiphoton absorption process as shown in **Figure 11**. In practice this is often realized by two-photon absorption using photons at twice the wavelength needed for the transition. Using

multiphoton fluorescence has several advantages compared to single-photon fluorescence microscopy. First, light with lower energy can penetrate deeper into tissue. Second, it is intrinsically confocal, since only in the focal volume, the nonlinear two-photon absorption takes place, such that spatial filtering is obsolete. Moreover, it allows an even smaller active focal region, enhancing the axial resolution and further reducing background light compared to confocal fluorescence microscopy.^[123] As a disadvantage, ultra-short laser pulses need to be employed in order to drive the excitation and the fluorescence quadratically depends on the excitation intensity.

In 1997, Teich and Saleh made a very auspicious proposal how to overcome the above mentioned drawbacks of two-photon fluorescence microscopy (TPFM) by exploiting entangled photon pairs.^[14] Signal and idler photon pairs from SPDC are generated at the same time. Sending such pairs to fluorophores can lead to two-photon absorption and subsequent fluorescence. **Figure 12** shows the principal experimental setting envisioned in ref. [14]. This approach promises several advantages compared to the classical case: i) The operation in the single photon regime minimizes phototoxicity and photobleaching, which renders this method ideal for biochemical photosensitive samples. ii) In this quantum scenario, the two-photon absorption rate, and thus, the fluorescence intensity, scales linearly with the incoming photon flux. iii) While in the classical regime laser-power fluctuations lead to a varying active absorption region, photon pair fluorescence microscopy is independent from that. iv) The implementation can entirely rely on cw laser sources avoiding the deployment of expensive pulsed laser systems. Furthermore, it allows a much more compact design with smaller footprint and at lower costs. v) Since signal and idler photons are spectrally anticorrelated, the linewidth of their sum is given by the pump laser, samples with narrow two-photon absorption spectra can be investigated very efficiently.

Naturally, the question arises why there is no quantum version of a laser-scanning microscope yet, utilizing photon-pair absorption. The major issue is photon loss in the sample together with fairly small photon-pair rates. While in the classical case photons are absorbed according to Lambert's law with an absorption coefficient γ , a photon pair is absorbed at rate γ^2 . This is due to the fact that if either of the two photons is annihilated,

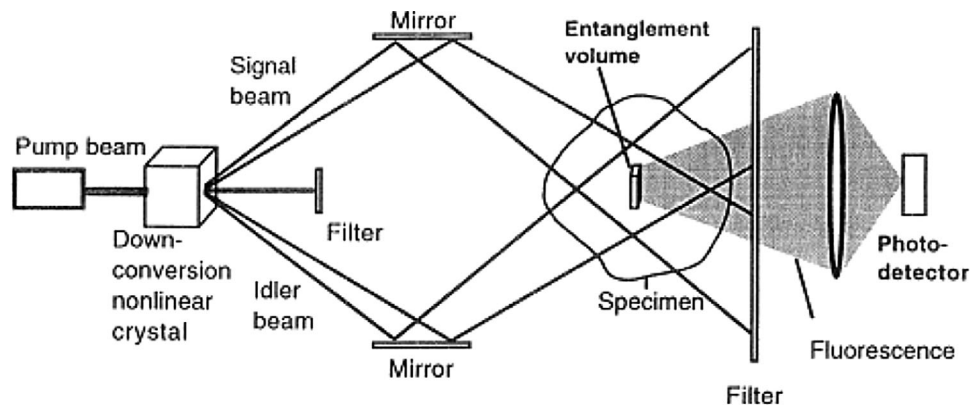


Figure 12. Photon-pair fluorescence microscopy. Photon pairs are generated by spontaneous parametric downconversion in a nonlinear crystal. Each of the twin beams is then steered into the sample. In the volume of spatial (and time) overlap linearly responding photon-pair absorption drives the fluorescence. Reproduced with permission.^[14] Copyright 1997, Fizikalni Ustav Akademie Ved Ceske Republiky.

the partner photon cannot be used and the whole photon pair is lost. Hence, the penetration depth into tissue is reduced by a factor of $1/\gamma$. Nevertheless, since the initial proposal several experiments in this direction had been carried out successfully.^[124–128] Yet, all of them suffer from the rather low pair generation rate in the BBO crystals used for photon-pair generation. However, photon pair sources based on SPDC in periodically poled crystals (e.g., ppKTP) not only allow a broader variety in wavelength selection but also tremendously enhance the photon pair rate to 1×10^6 counts per mW pump power,^[59,129] which can be further increased by at least an order of magnitude by employing waveguide structures within the periodically poled non-linear crystals.^[130,131]

As one can see, newly developed SPDC sources enable fairly high photon pair rates that are sufficient to enable photon pair fluorescence microscopy, in particular in combination with an intense pump laser.^[132,133] One of the main obstacles in the way for implementation clearly is the dispersion control of the signal and idler photons, which is needed to ensure their simultaneous arrival in the sample. Dispersion control becomes even more crucial when taking the broad individual spectra of signal and idler into account, which is necessary for a sufficient high pair rate. Naturally, an open task remains for the integration of such sources in order to provide stable turn-key photon pair sources at small footprint and to implement a specific microscopic design and demonstrate its feasibility for biomedical imaging. A first benchmarking test will be the clear demonstration of the linear response in an actual fluorescent biomarker.

5.2. Quantum Interference Microscopy

As we already saw in Section 3, interferometric structures can be applied in the quantum domain for imaging and spectroscopy. One of the key usages of interferometers is sensing. To this end, let us briefly recapitulate the working principle of the MZI in case of classical laser light. An incoming laser beam will be coherently split at a 50:50 beam splitter. If the MZI is balanced, both beams travel exactly the same optical path length and interfere at a second 50:50 beam splitter. One of the output port stays dark due to destructive interference, the other one contains all the emerging light. Making the MZI imbalanced by introducing a longer optical path in one of the arms, for example, by inserting a phase object with a phase delay θ , both output ports will contain light with the intensity $\approx \cos^2 \theta$ and $\approx \sin^2 \theta$, respectively. This way, a MZI can be applied for measuring path length differences, for example, caused by a substance with a specific density in the beam path. In doing so, the measurement uncertainty of the phase θ is given by $\Delta\theta = 1/\sqrt{\bar{n}} |\sin \theta|$, where \bar{n} is the average number of photons, which is directional proportional to the laser intensity.^[7,9] It is bounded by the shot-noise limit $\Delta\theta_{\text{SQL}} = 1/\sqrt{\bar{n}}$ for θ equal to odd multiples of $\pi/2$. This limit is also known as the standard quantum limit. The same approach holds true when exploiting M single photons (Fock states) instead of coherent laser light; intensities are replaced by probabilities and $\bar{n} = M$.

However, as shown below, this is not the minimum precision in phase estimation that is achievable. To this end, let us elaborate on the scenario, where the MZI is fed by two indistinguish-

able photons—one in each input port of the first beam splitter. Hence, the input state reads as $|1, 1\rangle$. Due to the Hong–Ou–Mandel (HOM) effect,^[134] the state after the first beam splitter will be $(|2, 0\rangle + |0, 2\rangle)/\sqrt{2}$. This means, both photons travel either the upper path in the MZI or the lower one. Due to this coherent superposition, a phase difference θ between the two path possibilities can be registered from coincidence measurements of the two output ports, as shown in **Figure 13**. At this point, the coincidence rate is proportional to $\approx \cos^2(2\theta)$ allowing measuring with a higher sensitivity compared to the scenario with single photons or coherent laser light. This was shown experimentally in ref. [135] using an interferometer with two SPDC crystals, one in each arm, that were coherently pumped by a pump laser split on the initial beam splitter. A natural generalization would be interferometry with N photons taking either the upper path or the lower. Along these lines, a phase shift θ would yield the N00N state $(|N, 0\rangle + e^{iN\theta} |0, N\rangle)/\sqrt{2}$. Accordingly, the sensitivity would be further enhanced. Moreover, the measurement uncertainty is given by the Heisenberg limit ($\bar{n} = N$)

$$\Delta\theta_{\text{HL}} = \frac{1}{\bar{n}} = \frac{1}{\sqrt{\bar{n}}} \Delta\theta_{\text{SQL}} \quad (13)$$

which improves on the shot noise limit by a factor of $1/\sqrt{\bar{n}}$.

This approach has many potential use cases, as interferometry can be performed below the shot noise limit, which has applications in ultraprecised measurement systems as, for example, gravitational wave detection systems.^[11–13,136] Furthermore, N00N state lithography promises smaller and more precise nanostructures.^[137] But as appealing this concept is, it has some severe practical limitations. Generating N00N states with $N > 2$ is a highly challenging task and today's limit is at $N = 7$.^[119] Keeping this in mind one can directly compare the performance of the laser MZI with the quantum MZI.

As we saw above, in the quantum MZI the average photon number is at today's maximum $\bar{n} = N \leq 7$, whereas in the classical laser MZI, the average photon number is determined by the laser intensity and thus, can be very high. Exactly for that reason, we do only see application of N00N state interferometry when the state preparation can be realized with sufficiently large number of photons.

Nevertheless, it is worth to mention another application of N00N states in form of an entanglement-enhanced microscope as presented by Ono et al.,^[138] schematically depicted in **Figure 14**. There, polarization N00N states were employed for differential interference contrast microscopy. The state was generated via two crossed type-I phasematched BBO crystals pumped at 405 nm. After passing through a calcite beam displacer, the following quantum state was realized: both photons are either in spatial mode a with horizontal polarization or in spatial mode b with vertical polarization (see **Figure 14**). A SNR enhanced by a factor of 1.35 ± 0.12 was demonstrated for a given average photon number of $\bar{n} = N = 2$. A similar work by Israel et al. demonstrated the feasibility for $N = 3$.^[139] However, while both schemes are beautiful proof-of-principle experiments they are limited by $N \leq 3$. The obtained SNR benefit will be of limited significance for many applications, albeit the increased sensitivity allows the investigation of samples with very low differential contrast.

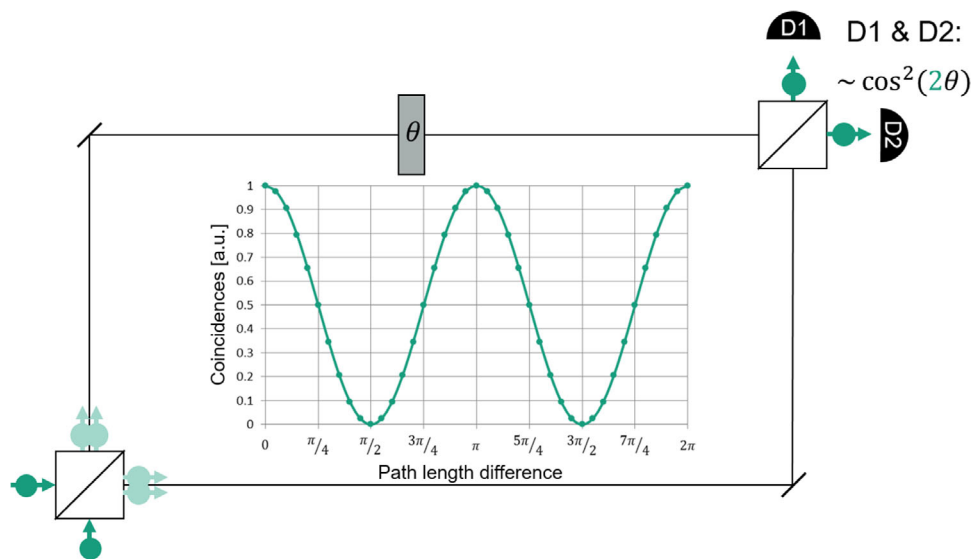


Figure 13. Mach-Zehnder interferometer with N00N states. Two indistinguishable photons impinge on a first beam splitter, one in each port, and are transferred into a N00N state according to the Hong–Ou–Mandel effect.^[134] Coincidence measurements of the output ports of the second beam splitter oscillate at $2q$, when q is the path-length difference between the interferometer arms.

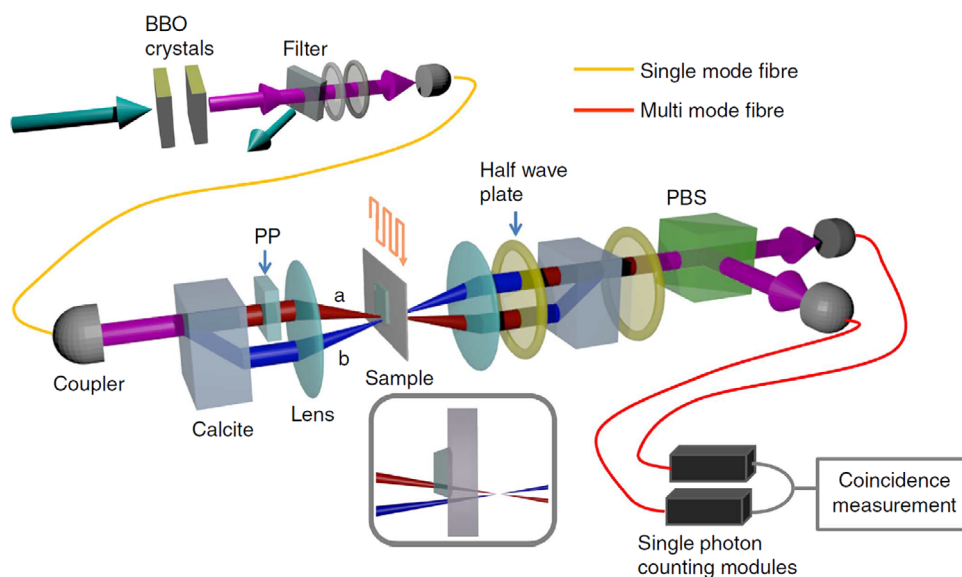


Figure 14. Entanglement-enhanced microscope. Polarization N00N states are utilized to implement a polarization differential-interference microscope. PP = phase plate and PBS = polarizing beam splitter. Opposite linear polarization states are shown by the blue and red beam, respectively. Reproduced with permission.^[138] Copyright 2013, Springer Nature.

As a concluding remark, we would like to mention also another, closely related line of research that makes use of two-photon interference. When two identical photons impinge simultaneously on a beam splitter, they both leave the beam splitter through a common output port, resulting in a characteristic HOM dip in the coincidence count rate. The HOM effect^[134] can be used to measure optical delays between different paths, as was already noted in the seminal 1987 paper by Hong, Ou, and Mandel. This feature lies at the heart of what has now become known as HOM interferometry and was recently used in a series of HOM-based time delay sensors with a wide dynamic range^[140]

and novel protocols such as quantum optical coherence tomography (QOCT).^[141]

6. Quantum Imaging Device Development

6.1. Source Development

Quantum light sources are continuously advancing and devices such as single-photon emitters and entangled photon pair sources may now be considered standard tools in quantum

optics laboratories around the world. Nevertheless, they are still predominantly bulky optical setups which are generously dimensioned to allow for easy addition of optical components and often feature redundant degrees of freedom for performance optimization. This comes at the cost of reduced reliability and makes constant performance monitoring and maintenance an absolute necessity. Much like in the early days of laser research, users require expert knowledge of the particular sources' inner workings to ensure reliable operation. For quantum light source to find wide-range application in the fields of biology and medical imaging, it will be necessary to advance from proof-of-concept demonstrators to compact, cost-efficient devices with reliable turn-key operation, comparable to present-day commercial laser systems.

Some of the main engineering challenges toward this vision include miniaturization of sources and the elimination of redundant degrees of freedom to facilitate improved long-term performance stability, as well as standardized interfaces that will allow for modular integration into microscopy systems. For such applications to be commercially viable, it will also be necessary to reduce the number, cost, and complexity of optical components required to build the source and to develop scalable manufacturing procedures. In this context, recent progress toward fully integrated quantum photonic platforms, promising fully integrated solutions, could play an important role.^[142–145]

To generally boost their optical performance, researchers are continuously improving quantum sources respect to every possible degree of freedom: broadening the range of accessible wavelengths, increasing photon yield, engineering quantum states with desirable spectral and spatial properties at near perfect state fidelity, as well as tailored photon number distributions.

The development of nonlinear crystals with a large aperture is a key requirement toward high-resolution quantum imaging applications.^[44] Furthermore, since the crystal length affects the spatial correlations of biphotons, these crystals should be of limited thickness.^[2] Hence, to achieve a significant photon flux, the crystals must thus also exhibit a large nonlinearity. At present, aperture sizes for commercially available periodically poled nonlinear crystals are approximately 1–2 mm.^[59,129] Engineering uniform periodically poled nonlinear crystals with significantly larger apertures is a key challenge. To this end, recent reports on high optical nonlinearities in few-layer and even monolayer crystals also indicate a promising line of future research.^[146]

With regards to operational wavelength ranges, we must distinguish between the requirements for two main types of imaging schemes: those that require photons to be generated at a single operational wavelength (e.g., NOON state microscopy) and those that allow for, or even require, non-identical wavelengths of photons (e.g., imaging with undetected photons, ghost imaging).

In the case of NOON state microscopy, for example, short-wavelength PDC sources are beneficial as they maximize optical path length sensitivity. However, the majority of efficient PDC sources demonstrated to date generate photons in the near infrared, as required for low-loss transmission via long-distance communication channels in free space and fiber. Operation in the visible wavelength range usually involves nonlinear frequency conversion.^[147] While first pair sources at wavelengths around 532 nm have already been demonstrated, the pair generation efficiency that are still prohibitively low for many applications. This

is, in part, due to the fact that the short pump wavelengths required to produce photon pairs at such short wavelengths are below the absorption edge of many commonly used nonlinear materials. As outlined in the introductory sections, the majority of efficient SPDC sources demonstrated to date are based on quasi-phase matching in periodically poled ferroelectric crystals and waveguides (KTP, LN) which are not transparent at pump wavelengths less than ≈ 350 nm. Ongoing research into novel nonlinear materials as well as efficient cavity-enhanced frequency conversion schemes would extend the range of wavelengths accessible via SPDC, and with it the scope of potential applications.

Arguably the most significant ongoing challenge with regards to quantum microscopy relates to the generation of higher-order NOON states. While such states may be generated via interference of quantum states and coherent light on a beam splitter,^[148] improvements in the total emission numbers are still required. Moreover, in the long run, it seems likely that the need for deterministic photon guns in quantum computation and quantum networks will also drive development of deterministic Fock state emitters suitable for quantum imaging, such as quantum dots, solid state emitters, atomic ensembles, or single atoms and ions.

With regards to quantum imaging with undetected photons, it can be desirable to produce signal and idler fields at significantly different wavelengths. In particular, a number of applications would benefit from extending the lower-energy (idler) photon into the mid-IR. Typical nonlinear materials, such as LN and KTP, provide access to SPDC wavelengths from ultraviolet to near infrared. SPDC in bulk ppLN^[6] as well as ppLN waveguides^[149] have already been used to generate non-degenerate wavelength combinations with the signal in the visible and the idler at 4–5 μm . However, significantly longer wavelengths cannot be achieved due to the limited transparency range of these materials.

To significantly extend this range into the THz will require further advances in nonlinear material engineering, whereby a number of potential candidate materials (e.g., orientation-patterned [OP] GaP, OP-GaAs) with transparency ranges that extend well into the mid-IR have already been identified. The reader is referred to ref. [150] for a detailed discussion of long-wavelength SPDC and candidate materials. A first attempt toward the THz regime was announced just recently.^[151]

The generation of short-wavelength photons in the deep UV range poses an even bigger engineering challenge. At wavelengths below 350 nm currently used periodically poled nonlinear crystals such as ppKTP and ppLT become opaque. Shorter-wavelength PDC can be achieved via BPM in BBO (UV cut-off 190 nm) at the cost of reduced efficiency and flexibility compared to QPM interactions. Results on SPDC from X-rays to XUV^[152,153] demonstrate that even more extreme SPDC configurations are indeed possible, and the reader is referred to ref. [154] for an account of recent activities in the field of X-ray quantum optics.

6.2. Feasible Detection Systems

The detection of single photons is essential for the discussed quantum imaging schemes. Although it is a challenging task,

especially when considering photon pair coincidence detection, huge technical developments have been achieved in the field of single photon detectors. A full review of all different types is beyond the scope of this work. Therefore, we would like to mention a review by Hadfield on single photon detectors for quantum information covering many of the different detector types.^[155] Naturally, the detectors described there are single pixel detectors. For quantum imaging, one needs to apply them in a scanning way (e.g., by a scanning fiber tip) or in an engineered 2D array form.

In the following, we are going to present the most common detection systems very briefly, mention their strengths, weaknesses, and discuss their suitability for quantum imaging applications.

6.2.1. Avalanche Photodiodes

Single photon avalanche photodiodes (SPADs) are diodes operated in reverse voltage mode and exploiting an avalanche multiplication as gain of the photoelectric effect. They are the most commonly used detector in the quantum photonic community, since they are relatively cheap, and have a moderate detection efficiency of up to $\approx 80\%$ in the VIS range. However, in other spectral regions, especially for longer wavelengths, silicon cannot be used as detector material and APDs suffer from enhanced noise. Furthermore, they are not photon number resolving. Interestingly, they can be built in 2D SPAD-arrays currently of up to 265×256 pixels^[156] where each pixel is a SPAD.^[157–159] This offers applications for coincidence imaging^[160] but the pixel number is still fairly low. Due to the electronics around the actual sensitive area, the filling factor is low, too. Hence, the overall detection efficiency is lowered. Applying microlens arrays might be a potential way to counter this issue.

6.2.2. Superconducting Nanowires

A superconducting nanowire single photon detector (SNSPDs) consists of a meandered nanowire made, for example, from Niobium, which is superconducting. When a photon hits the nanowire, it locally breaks many Cooper pairs. Thus, the nanowires become normal conductors and an electrical signal can be measured. This way single photons in the VIS and NIR can be detected with $> 85\%$ detection efficiency.^[161–163] However, SNSPDs can also be used for much longer wavelengths up to $5 \mu\text{m}$ ^[162] although the efficiency still needs to be optimized. Similar to SPADs, they allow detection rates in the MHz range. Typical SNSPDs need operating temperatures below 4 K, which can be reached with closed-cycle helium cryostats that can be operated without particular additional infrastructure. Developed only in 2001, SNSPDs are already commercially available, however, rather expensive. As recent research results indicate, they can in principle resolve photon numbers,^[164,165] but as of now there is no practicable and commercially available implementation using this capability. The same holds true for achieving 2D spatial resolution^[166] or the arrangement as 1D detector array.^[167,168]

6.2.3. Transition Edge Sensors

Transition edge sensors (TES) are highly-sensitive bolometers built by a superconducting film (e.g., made of Tungsten) and are operated near the superconducting transition temperature.^[169,170] When a photon hits the film, its energy causes an increase in the electrical resistance. Intriguingly, the energy of the absorbed quantum particle(s) is proportional to the resistance change. Therefore, TES are capable of photon number resolving. In addition, their second strength is their eminently high detection efficiency $\approx 95\%$ at telecom wavelengths. On the downside, their count rate is two to three orders of magnitude below the ones from SPADs and SNSPDs, they commonly run at temperatures of ≈ 100 mK which is not easily achievable and they are not commercially available. In essence, TES arrays are very suitable for fundamental research in quantum information and in astronomy but due to their low operation temperature, most probably will not become the detector of choice for applicable quantum imaging.

6.2.4. Intensified Charge-Coupled Device

An intensified charge-coupled device (ICCD) is a CCD equipped with an light intensifying element (e.g., a microchannel plate) in front of it. This way any incoming signal will be intensified before hitting the CCD chip, where it is read out. ICCDs allow single photon detection with currently up to $\approx 50\%$ detection efficiency at a very low dark count level. Furthermore, the intensifier can be gated for very short times in the ns range, making these cameras suitable for photon correlation experiments. Hence, ICCDs were already massively harnessed for quantum imaging research; for instance, detection of spatial correlations of SPDC photon pairs,^[171] ghost imaging,^[78,97,101] and few photon imaging.^[82] Nevertheless, as the final detection is still based on a comparably slow CCD or CMOS sensor, measurements of the photon arrival time are not possible. Furthermore, the quantum efficiency is still low compared to EMCCD or sCMOS sensors, hence the advantages of QGI cannot be fully used.

6.2.5. Electron Multiplying Charge-Coupled Device

In contrast to ICCDs, EMCCDs perform the intensification after the detection of light on a CCD. An electron multiplying register provides the gain of the detected electronic signal. Therefore, EMCCDs have a higher detection efficiency than ICCDs and a lower readout noise. However, their overall SNR is in general worse compared to ICCDs since dark counts are intensified as well. Additionally, they need to be cooled, but are less expensive. EMCCDs are commonly used in quantum imaging experiments, too. Examples are subshot-noise correlation measurements and imaging,^[84,172] entanglement detection by Einstein–Podolsky–Rosen experiments,^[173–176] and quantum imaging with undetected photons.^[5,65]

6.2.6. Scientific Complementary Metal-Oxide Semiconductor

A scientific complementary metal-oxide semiconductor (sCMOS) is a hybrid technology between CCD and CMOS

technology. In CMOS chips, each pixel is composed of a photodiode amplifier pair, such that the readout of each pixel is not serial (as for CCD), but in parallel. This allows much faster readouts. In case of a sCMOS, the CMOS readout circuit is bump bonded to a CCD substrate. This way, sCMOS cameras offer a very low noise level, fast readout, and high detection efficiency. Additionally, they are much cheaper than EMCCDs or ICCDs. Since the technology is fairly new, there are no explicit quantum-enhanced imaging experiments yet. Nevertheless, there are plenty of experimental applications of low light imaging at high quality level.^[177–179]

6.2.7. Photon Frequency Upconversion

A very different way to detect photons at wavelengths (e.g., IR) where no efficient and affordable detector is available is its frequency upconversion toward the VIS range.

An ideal frequency converter shifts the carrier frequency of the probe beam while preserving the spectral and spatial properties. To this end, parametric frequency-conversion in nonlinear materials offers several suitable possibilities, such as difference-frequency conversion, second harmonic generation, sum frequency generation, and four wave mixing.

In particular, efforts toward image-preserving frequency conversion^[180–183] and amplification^[184,185] are being pursued by numerous nonlinear optics groups around the world. With recent advances in imaging based on structured illumination,^[186] the development of suitable frequency converters^[187] and mode analyzers^[188,189] could also extend the wavelength range for coherent imaging schemes based on structured wave fronts.

A number of experimental implementations have also demonstrated this principle and verified that even correlations and entanglement can be preserved.^[190–195] Quantum frequency conversion, which is driven primarily by that task of bridging wavelengths for transmission over distance and storage in quantum memories will play a crucial role in future quantum communication networks.

However, reaching the conversion efficiency sufficient for practical usage necessitates the use of high-Q cavities that restrict both the frequency and spatial spectrum of the converted photons. A recent advance in this direction was the frequency-conversion of spatial quantum information via SFG in a suitably designed optical cavity. This way, researchers were able to achieve quantum conversion efficiencies of 0.224, 0.0833, and 0.0296 for structured single-photon beams with a topological charge of $l = 0, 1, 2$, respectively.^[196]

However, further advances in the conversion efficiency and modal bandwidth will still have to be achieved, for this approach to become practical in quantum imaging or spectroscopy applications.

6.2.8. Summary

Naturally, there are many ways to detect single photons and the choice of the detector strongly depends on the specific application. Very sophisticated technologies like SNSPDs and TES are not very practicable for actual quantum-enhanced imaging de-

vices. When it comes to imaging via coincidence detection (e.g., ghost imaging), SPAD arrays are the detector of choice. While they are already commercially available, they need a lot of improvement concerning number of pixels, detection efficiency and the ability to practically correlate all pixels with each other. On the contrary, ICCDs, EMCCDs, and sCMOS cameras are already in use for quantum imaging setups and especially sCMOS cameras offer a very good trade-off between performance, footprint, and price, and thus, are a very promising candidate to be implemented in upcoming devices. Although all three of them work pretty well in the VIS, they cannot detect in the mid-IR. In particular for IR image detection, we see plenty of room for technical development—either on the side of InGaAs SPAD cameras or to have affordable SNSPD-based imaging devices. However, as presented in this review, there are novel schemes to circumvent IR detection and there are many application where the detection is actually desired in the VIS.

In general, we see the demand for technical improvements in particular in the realm of coincidence detection. Here SPAD-arrays with larger pixel numbers in both dimension as well as higher filling factors are necessary to allow the practical utilization of various QGI schemes. For quantum imaging approaches not relying on coincidence detection, we see the main need for improvements more on the actual quantum imaging schemes rather than on the detection side. The established detection technologies are already very mature there, whereas the quantum imaging schemes just started to be transferred from pure academic setups into commercially available devices.

6.3. Algorithms for Image Improvement or Reconstruction

For many applications of quantum imaging, especially QGI, one main aim is the reduction of the illumination intensity on the measured object, that is, the collection of images with photon numbers as small as possible. Whereas in classical imaging, typically several thousand photons per image pixel are used, QGI has been shown with only a few tens of photons per pixel. However, such images appear very noisy due to the noise associated with a finite number of photon detection events and the resulting pixel-to-pixel variations. Although this noise is lower than in classical imaging with the same number of photons, practical applications of quantum imaging modalities will require improvement of the image quality. This can of course be reached by simply using more photons. On the other hand, there already exist sophisticated numerical algorithms that allow to reconstruct images from very low numbers of photons.

These algorithms make use of the fact that the noise in the individual pixels is known to be Poissonian and that the spatial spectrum of real images is usually sparse, that is, their spatial intensity distribution is not just a random arrangement but correlations between neighboring pixels exist. Using this a priori knowledge, numerical algorithms have been developed that calculate a reconstructed image by minimizing the sparsity in the spatial spectrum while staying consistent with the measured data taking into account the known noise model.^[197] This led to the measurement of images with on average, less than one photon per image pixel.^[82] Similar algorithms have been already applied for photon-efficient classical imaging.^[198] However, as has been discussed

before, the SNR of the measured data can be inherently better for quantum imaging schemes based on correlation measurements, especially for low photon numbers. Consequently, this will lead also to an improved accuracy of the reconstructed image.

7. Summary and Outlook

We have presented various quantum imaging techniques and categorized them in three topics: interference-, correlation-, and entanglement-based quantum imaging. As it becomes clear several quantum imaging techniques are available and some show great potential for practicable application within a near future term. We would like to emphasize three very promising approaches.

One is the interference-based quantum imaging. It is very attractive since the sample interaction and the actual light detection is carried out by different photons that can have quite different center wavelength. Hence, new spectral ranges can be imaged by still employing standard silicon-based cameras optimized for the VIS. Hence, it allows to use well-established, good-performing, and economic cameras. In particular, we see application within the fields of IR microscopy and THz imaging, which could now be carried out in a nonlinear interferometer with VIS detectors. Furthermore, UV or deep UV microscopy becomes attractive again, since it features a high contrast for biomolecules and due to the single photon level combined with the high detection efficiency in the VIS, phototoxicity can be brought to a minimum level. Again, high-efficient detection in the VIS can be applied. However, in order to become a feasible technique for life science labs several improvements are necessary. First, imaging setups need to become more compact and stable. In Section 3.2, we already pointed out, that a single crystal scheme promises a much smaller footprint, better visibility, and more stability. Together with system integration, such setups can turn into applicable devices and demonstrators. Second, especially for UV imaging, further photon pair source development needs to be done. Due to energy conservation SPDC might not be the process of choice for that direction. Spontaneous four wave mixing can be an expedient. Its successful application for photon pair generation was already demonstrated,^[20,22,199–202] but more progress with respect to imaging applications involving UV light needs to be done.

Quantum ghost imaging and spectroscopy seems promising for two different applications. First, for transmissive or reflective imaging of very photonsensitive objects, where the fundamentally possible gain in SNR possible with QGI could enable further reduction of the photon dose compared to microscopy schemes used now. Second, advantages can be expected when using the fact that the propagation between the object and the bucket detector does not need to preserve coherence. This means that scattering or other noise in this part of the imaging system does not deteriorate the image. For reflective QGI in a scattering or noisy environment, where light is impinging on an object and then coming back to a detector, this means that the distance to the object can be increased with respect to classical imaging. This may find applications in the automotive technologies that aim at imaging through fog or rain, or in biological imaging through scattering tissue. This advantage can be further enhanced by using longer

wavelengths, where the imaging with the spatially resolving detector can still be done in the visible spectral range. However, actual applications of QGI are currently hampered by the lack of ideal detectors. Bucket detectors are available with sufficient efficiency only in the visible and near-infrared spectral ranges, where APDs and SNSPDs have their highest efficiencies. Efficient camera systems, which only need to be in the visible, do not yet provide the capability for photon timing and correlation. On the other hand, imaging detectors composed from SPADs, which have a high potential if their efficiencies are further raised, do not yet provide a large spatial resolution.

As another technique very close to be harnessed in near future, we identify the entangled TPFM (see Section 5.1). It comes with all the advantages that TPFM offers except of the intrinsic confocality. However, if necessary, this can be countered by the additional utilization of a photo activating light sheet to select different depth layers. Moreover, the application of entangled photon pairs allows for smaller foci. But the by-far biggest advantage is the linear dependence of the fluorescence signal on the illumination intensity. Here, we see a clear application field for low light imaging of photosensitive tissue or processes. Ideally, only the illumination part of already established laser scanning microscopes needs to be replaced by a proper photon pair source. Nevertheless, this includes the main challenge: the proper photon pair source. In order to drive detectable fluorescence a photon pair flux in the order of several $\mu\text{W-mW}$ is required. Taking the quadratic loss rate of photon pairs into account, this can become a challenging task. Keeping SPDC as the process of choice here, the downconverted photon stream need to stay non-classical. This means that much higher pump powers leading to a high-gain downconversion is not suitable. However, that are mainly the only harsh restrictions to the photon pair source. The photons can be spectrally very broad and carried in one optical mode. Hence, sophisticated illumination techniques, large aperture crystals, and nonlinear waveguide structures or a combination could lead to significantly enhanced brightness of photon pair source suitable for entangled TPFM.

In summary, the current challenge is the transfer of the quantum imaging concepts described in this review, which up to now are all fundamentally understood and demonstrated, toward real-life applications. As can be seen from the selected examples, based on the current state of the art, the development of quantum-enhanced imaging may be especially beneficial for life sciences. However, it is expected that further improved quantum imaging modalities may find application also in other areas.

Acknowledgements

This article is part of a special series highlighting advances in quantum science and technology. This work was supported as a Fraunhofer LIGHTHOUSE PROJECT (QUILT) and by the Fraunhofer Attract program (QCtech). Furthermore, funding from the German Federal Ministry of Education and Research (BMBF) under the project identifiers 03ZZ0434 and 13N14877 as well as from the German Research Foundation (DFG) under project identifier SE 2749/1-1 is acknowledged.

Conflict of Interest

The authors declare no conflict of interest.

Keywords

entangled photon pairs, ghost imaging, quantum imaging, quantum microscopy

Received: March 15, 2019

Revised: May 29, 2019

Published online: September 10, 2019

- [1] R. Boyd, D. Prato, *Nonlinear Optics*, Elsevier Science, Oxford, UK **2008**.
- [2] C. Couteau, *Contemp. Phys.* **2018**, *59*, 291.
- [3] M. H. Rubin, Y. Shih, *Phys. Rev. A* **2008**, *78*, 033836.
- [4] S. Karmakar, Y. Shih, *Phys. Rev. A* **2010**, *81*, 033845.
- [5] G. B. Lemos, V. Borish, G. D. Cole, S. Ramelow, R. Lapkiewicz, A. Zeilinger, *Nature* **2014**, *512*, 409.
- [6] D. A. Kalashnikov, A. V. Paterova, S. P. Kulik, L. A. Krivitsky, *Nat. Photonics* **2016**, *10*, 98.
- [7] R. Loudon, *The Quantum Theory of Light*, Oxford University Press, Oxford, UK **2000**.
- [8] N. Treps, N. Grosse, W. P. Bowen, C. Fabre, H. A. Bachor, P. K. Lam, *Science* **2003**, *301*, 940.
- [9] C. Gerry, P. Knight, *Introductory Quantum Optics*, Cambridge University Press, Cambridge, UK **2005**.
- [10] N. Samantaray, I. Ruo-Berchera, A. Meda, M. Genovese, *Light: Sci. Appl.* **2017**, *6*, e17005.
- [11] R. Schnabel, N. Mavalvala, D. E. McClelland, P. K. Lam, *Nat. Commun.* **2010**, *1*, 121.
- [12] T. L. I. G. O. S. Collaboration, J. Abadie, B. P. Abbott, R. Abbott, T. D. Abbott, M. Abernathy, C. Adams, R. Adhikari, C. Affeldt, B. Allen, G. S. Allen, E. A. Ceron, D. Amariutei, R. S. Amin, S. B. Anderson, W. G. Anderson, K. Arai, M. A. Arain, M. C. Araya, S. M. Aston, D. Atkinson, P. Aufmuth, C. Aulbert, B. E. Aylott, S. Babak, P. Baker, S. Ballmer, D. Barker, B. Barr, P. Barriga, et al., *Nat. Phys.* **2011**, *7*, 962.
- [13] H. Grote, K. Danzmann, K. L. Dooley, R. Schnabel, J. Slutsky, H. Vahlbruch, *Phys. Rev. Lett.* **2013**, *110*, 181101.
- [14] M. Teich, B. Saleh, *Cesk. Cas. Fyz.* **1997**, *47*, 3.
- [15] B. Lounis, M. Orrit, *Rep. Prog. Phys.* **2005**, *68*, 1129.
- [16] R. H. Hadfield, *Nat. Photonics* **2009**, *3*, 696.
- [17] M. D. Eisaman, J. Fan, A. Migdall, S. V. Polyakov, *Rev. Sci. Instrum.* **2011**, *82*, 071101.
- [18] L. Caspani, C. Xiong, B. J. Eggleton, D. Bajoni, M. Liscidini, M. Galli, R. Morandotti, D. J. Moss, *Light: Sci. Appl.* **2017**, *6*, e171100.
- [19] A. S. Solntsev, A. A. Sukhorukov, *Rev. Phys.* **2017**, *2*, 19.
- [20] K. Garay-Palmett, A. B. U'Ren, R. Rangel-Rojo, R. Evans, S. Camacho-López, *Phys. Rev. A* **2008**, *78*, 043827.
- [21] K. Garay-Palmett, D. Cruz-Delgado, F. Dominguez-Serna, E. Ortiz-Ricardo, J. Monroy-Ruz, H. Cruz-Ramirez, R. Ramirez-Alarcon, A. B. U'Ren, *Phys. Rev. A* **2016**, *93*, 033810.
- [22] P. Kultavewuti, E. Y. Zhu, X. Xing, L. Qian, V. Pusino, M. Sorel, J. S. Aitchison, *Sci. Rep.* **2017**, *7*, 5785.
- [23] L. Mandel, *Opt. Lett.* **1979**, *4*, 205.
- [24] I. Aharonovich, D. Englund, M. Toth, *Nat. Photonics* **2016**, *10*, 631.
- [25] P. G. Kwiat, K. Mattle, H. Weinfurter, A. Zeilinger, A. V. Sergienko, Y. Shih, *Phys. Rev. Lett.* **1995**, *75*, 4337.
- [26] P. G. Kwiat, E. Waks, A. G. White, I. Appelbaum, P. H. Eberhard, *Phys. Rev. A* **1999**, *60*, R773.
- [27] P. Trojek, C. Schmid, M. Bourennane, H. Weinfurter, C. Kurtsiefer, *Opt. Express* **2004**, *12*, 276.
- [28] H. S. Poh, S. K. Joshi, A. Cere, A. Cabello, C. Kurtsiefer, *Phys. Rev. Lett.* **2015**, *115*, 180408.
- [29] A. Villar, A. Lohrmann, A. Ling, *Opt. Express* **2018**, *26*, 12396.
- [30] A. Valencia, G. Scarcelli, Y. Shih, *Appl. Phys. Lett.* **2004**, *85*, 2655.
- [31] S. Tanzilli, H. De Riedmatten, W. Tittel, H. Zbinden, P. Baldi, M. De Micheli, D. B. Ostrowsky, N. Gisin, *Electron. Lett.* **2001**, *37*, 26.
- [32] S. Tanzilli, A. Martin, F. Kaiser, M. P. De Micheli, O. Alibart, D. B. Ostrowsky, *Laser Photonics Rev.* **2012**, *6*, 115.
- [33] M. Förtsch, J. U. Fürst, C. Wittmann, D. Strekalov, A. Aiello, M. V. Chekhova, C. Silberhorn, G. Leuchs, C. Marquardt, *Nat. Commun.* **2013**, *4*, 1818.
- [34] C. E. Kuklewicz, M. Fiorentino, G. Messin, F. N. Wong, J. H. Shapiro, *Phys. Rev. A* **2004**, *69*, 013807.
- [35] M. Fiorentino, S. M. Spillane, R. G. Beausoleil, T. D. Roberts, P. Battle, M. W. Munro, *Opt. Express* **2007**, *15*, 7479.
- [36] A. Fedrizzi, T. Herbst, A. Poppe, T. Jennewein, A. Zeilinger, *Opt. Express* **2007**, *15*, 15377.
- [37] G. Harder, V. Ansari, B. Brecht, T. Dirmeier, C. Marquardt, C. Silberhorn, *Opt. Express* **2013**, *21*, 13975.
- [38] F. Steinlechner, P. Trojek, M. Jofre, H. Weier, D. Perez, T. Jennewein, R. Ursin, J. Rarity, M. W. Mitchell, J. P. Torres, H. Weinfurter, V. Pruneri, *Opt. Express* **2012**, *20*, 9640.
- [39] E. Meyer-Scott, N. Prasannan, C. Eigner, V. Quiring, J. M. Donohue, S. Barkhofen, C. Silberhorn, arXiv:1807.10092 [quant-ph], **2018**.
- [40] R. W. Boyd, *Nonlinear Optics*, Elsevier, New York **2003**.
- [41] Y. Chen, S. Ecker, S. Wengerowsky, L. Bulla, S. K. Joshi, F. Steinlechner, R. Ursin, *Phys. Rev. Lett.* **2018**, *121*, 200502.
- [42] N. Gisin, G. Ribordy, W. Tittel, H. Zbinden, *Rev. Mod. Phys.* **2002**, *74*, 145.
- [43] V. Giovannetti, S. Lloyd, L. Maccone, *Nat. Photonics* **2011**, *5*, 222.
- [44] S. P. Walborn, C. Monken, S. Pádua, P. S. Ribeiro, *Phys. Rep.* **2010**, *495*, 87.
- [45] J. P. Torres, K. Banaszek, I. Walmsley, in *Progress in Optics* (Ed: E. Wolf), Elsevier, New York **2011**, pp. 227–331.
- [46] F. Just, A. Cavanna, M. V. Chekhova, G. Leuchs, *New J. Phys.* **2013**, *15*, 083015.
- [47] J. Schneckloch, J. C. Howell, *J. Opt.* **2016**, *18*, 053501.
- [48] J. Torres, A. Alexandrescu, L. Torner, *Phys. Rev. A* **2003**, *68*, 050301.
- [49] D. Ljunggren, M. Tengner, *Phys. Rev. A* **2005**, *72*, 062301.
- [50] A. Ling, A. Lamas-Linares, C. Kurtsiefer, *Phys. Rev. A* **2008**, *77*, 043834.
- [51] R. S. Bennink, *Phys. Rev. A* **2010**, *81*, 053805.
- [52] S. Palacios, R. d. J. León-Montiel, M. Hendrych, A. Valencia, J. P. Torres, *Opt. Express* **2011**, *19*, 14108.
- [53] B. E. Saleh, A. F. Abouraddy, A. V. Sergienko, M. C. Teich, *Phys. Rev. A* **2000**, *62*, 043816.
- [54] J. P. Torres, C. I. Osorio, L. Torner, *Opt. Lett.* **2004**, *29*, 1939.
- [55] J. C. Howell, R. S. Bennink, S. J. Bentley, R. Boyd, *Phys. Rev. Lett.* **2004**, *92*, 210403.
- [56] M. Ritsch-Marte, *Philos. Trans. R. Soc., A* **2017**, *375*, 20150437.
- [57] S. M. Barnett, M. Babiker, M. J. Padgett, *Philos. Trans. R. Soc., A* **2017**, *375*, 20150444.
- [58] W. P. Grice, R. S. Bennink, D. S. Goodman, A. T. Ryan, *Phys. Rev. A* **2011**, *83*, 023810.
- [59] F. Steinlechner, S. Ramelow, M. Jofre, M. Gilaberte, T. Jennewein, J. P. Torres, M. W. Mitchell, V. Pruneri, *Opt. Express* **2013**, *21*, 11943.
- [60] E. Meyer-Scott, N. Prasannan, C. Eigner, V. Quiring, J. M. Donohue, S. Barkhofen, C. Silberhorn, *Opt. Express* **2018**, *26*, 32475.
- [61] X. Y. Zou, L. J. Wang, L. Mandel, *Phys. Rev. Lett.* **1991**, *67*, 318.
- [62] L. J. Wang, X. Y. Zou, L. Mandel, *Phys. Rev. A* **1991**, *44*, 4614.
- [63] M. Lahiri, A. Hochrainer, R. Lapkiewicz, G. B. Lemos, A. Zeilinger, arXiv:1709.09974 [quant-ph], **2017**.
- [64] M. Lahiri, R. Lapkiewicz, G. B. Lemos, A. Zeilinger, *Phys. Rev. A* **2015**, *92*, 013832.
- [65] A. Hochrainer, M. Lahiri, R. Lapkiewicz, G. B. Lemos, A. Zeilinger, *Optica* **2017**, *4*, 341.
- [66] M. I. Kolobov, E. Giese, S. Lemieux, R. Fickler, R. W. Boyd, *J. Opt.* **2017**, *19*, 054003.

- [67] A. Paterova, H. Yang, C. An, D. Kalashnikov, L. Krivitsky, *New J. Phys.* **2018**, *20*, 043015.
- [68] M. A. Broome, M. P. Almeida, A. Fedrizzi, A. G. White, *Opt. Express* **2011**, *19*, 22698.
- [69] M. Takeoka, R. B. Jin, M. Sasaki, *New J. Phys.* **2015**, *17*, 043030.
- [70] A. Vallés, G. Jiménez, L. J. Salazar-Serrano, J. P. Torres, *Phys. Rev. A* **2018**, *97*, 023824.
- [71] A. Paterova, S. Lung, D. A. Kalashnikov, L. A. Krivitsky, *Sci. Rep.* **2017**, *7*, 42608.
- [72] A. S. Solntsev, P. Kumar, T. Pertsch, A. A. Sukhorukov, F. Setzpfandt, *APL Photonics* **2018**, *3*, 021301.
- [73] T. Pittman, D. Strekalov, D. Klyshko, M. Rubin, A. Sergienko, Y. Shih, *Phys. Rev. A* **1996**, *53*, 2804.
- [74] B. I. Erkmén, J. H. Shapiro, *Adv. Opt. Photonics* **2010**, *2*, 405.
- [75] J. H. Shapiro, R. W. Boyd, *Quantum Inf. Process.* **2012**, *11*, 949.
- [76] A. Meda, E. Losero, N. Samantaray, F. Scafirimuto, S. Pradyumna, A. Avella, I. Ruo-Berchera, M. Genovese, *J. Opt.* **2017**, *19*, 094002.
- [77] D. Strekalov, A. Sergienko, D. Klyshko, Y. Shih, *Phys. Rev. Lett.* **1995**, *74*, 3600.
- [78] D. Tasca, R. Aspden, P. Morris, G. Anderson, R. Boyd, M. Padgett, *Opt. Express* **2013**, *21*, 30460.
- [79] A. F. Abouraddy, P. R. Stone, A. V. Sergienko, B. E. Saleh, M. C. Teich, *Phys. Rev. Lett.* **2004**, *93*, 213903.
- [80] T. Pittman, Y. Shih, D. Strekalov, A. Sergienko, *Phys. Rev. A* **1995**, *52*, R3429.
- [81] R. S. Aspden, D. S. Tasca, R. W. Boyd, M. J. Padgett, *New J. Phys.* **2013**, *15*, 073032.
- [82] P. A. Morris, R. S. Aspden, J. E. Bell, R. W. Boyd, M. J. Padgett, *Nat. Commun.* **2015**, *6*, 5913.
- [83] P. A. Moreau, E. Toninelli, T. Gregory, M. J. Padgett, *Laser Photonics Rev.* **2018**, *12*, 1700143.
- [84] G. Brida, M. Genovese, I. R. Berchera, *Nat. Photonics* **2010**, *4*, 227.
- [85] E. Lopaeva, I. R. Berchera, I. Degiovanni, S. Olivares, G. Brida, M. Genovese, *Phys. Rev. Lett.* **2013**, *110*, 153603.
- [86] E. Jakeman, J. Rarity, *Opt. Commun.* **1986**, *59*, 219.
- [87] M. M. Hayat, A. Joobeur, B. E. Saleh, *JOSA A* **1999**, *16*, 348.
- [88] M. Li, C. L. Zou, D. Liu, G. P. Guo, G. C. Guo, X. F. Ren, *Phys. Rev. A* **2018**, *98*, 012121.
- [89] P. A. Moreau, J. Sabines-Chesterking, R. Whittaker, S. K. Joshi, P. M. Birchall, A. McMillan, J. G. Rarity, J. C. Matthews, *Sci. Rep.* **2017**, *7*, 6256.
- [90] G. Brida, M. Chekhova, G. Fornaro, M. Genovese, E. Lopaeva, I. R. Berchera, *Phys. Rev. A* **2011**, *83*, 063807.
- [91] S. Lloyd, *Science* **2008**, *321*, 1463.
- [92] S. H. Tan, B. I. Erkmén, V. Giovannetti, S. Guha, S. Lloyd, L. Maccone, S. Pirandola, J. H. Shapiro, *Phys. Rev. Lett.* **2008**, *101*, 253601.
- [93] J. H. Shapiro, S. Lloyd, *New J. Phys.* **2009**, *11*, 063045.
- [94] Y. Zhang, A. Sit, F. Bouchard, H. Larocque, F. Grenapin, E. Cohen, A. C. Elitzur, J. L. Harden, R. W. Boyd, E. Karimi, *Opt. Express* **2019**, *27*, 2212.
- [95] K. W. C. Chan, M. N. O'Sullivan, R. W. Boyd, *Phys. Rev. A* **2009**, *79*, 033808.
- [96] C. C. Kim, G. Kanner, presented at *Quantum Communications and Quantum Imaging VIII*, San Diego, CA, USA, August **2010**.
- [97] R. S. Aspden, N. R. Gemmill, P. A. Morris, D. S. Tasca, L. Mertens, M. G. Tanner, R. A. Kirkwood, A. Ruggeri, A. Tosi, R. W. Boyd, G. S. Buller, R. H. Hadfield, M. J. Padgett, *Optica* **2015**, *2*, 1049.
- [98] I. F. Santos, L. Neves, G. Lima, C. Monken, S. Pádua, *Phys. Rev. A* **2005**, *72*, 033802.
- [99] A. F. Abouraddy, B. E. Saleh, A. V. Sergienko, M. C. Teich, *JOSA B* **2002**, *19*, 1174.
- [100] M. Zhong, P. Xu, L. Lu, S. Zhu, *Sci. China: Phys., Mech. Astron.* **2016**, *59*, 670311.
- [101] P. A. Moreau, E. Toninelli, P. A. Morris, R. S. Aspden, T. Gregory, G. Spalding, R. W. Boyd, M. J. Padgett, *Opt. Express* **2018**, *26*, 7528.
- [102] S. Karmakar, R. E. Meyers, Y. Shih, *J. Biomed. Opt.* **2015**, *20*, 016008.
- [103] Z. Li, N. Medvedev, H. N. Chapman, Y. Shih, *J. Phys. B: At., Mol. Opt. Phys.* **2017**, *51*, 025503.
- [104] G. Scarcelli, A. Valencia, S. Gompers, Y. Shih, *Appl. Phys. Lett.* **2003**, *83*, 5560.
- [105] A. Yabushita, T. Kobayashi, *Phys. Rev. A* **2004**, *69*, 013806.
- [106] A. Kalachev, D. Kalashnikov, A. Kalinkin, T. Mitrofanova, A. Shkallikov, V. Samartsev, *Laser Phys. Lett.* **2007**, *4*, 722.
- [107] A. Kalachev, D. Kalashnikov, A. Kalinkin, T. Mitrofanova, A. Shkallikov, V. Samartsev, *Laser Phys. Lett.* **2008**, *5*, 600.
- [108] O. Slattery, L. Ma, P. Kuo, Y. S. Kim, X. Tang, *Laser Phys. Lett.* **2013**, *10*, 075201.
- [109] D. A. Kalashnikov, Z. Pan, A. I. Kuznetsov, L. A. Krivitsky, *Phys. Rev. X* **2014**, *4*, 011049.
- [110] D. Pelliccia, A. Rack, M. Scheel, V. Cantelli, D. M. Paganin, *Phys. Rev. Lett.* **2016**, *117*, 113902.
- [111] H. Yu, R. Lu, S. Han, H. Xie, G. Du, T. Xiao, D. Zhu, *Phys. Rev. Lett.* **2016**, *117*, 113901.
- [112] P. Zerom, K. W. C. Chan, J. C. Howell, R. W. Boyd, *Phys. Rev. A* **2011**, *84*, 061804.
- [113] P. B. Dixon, G. A. Howland, K. W. C. Chan, C. O'Sullivan-Hale, B. Rodenburg, N. D. Hardy, J. H. Shapiro, D. Simon, A. Sergienko, R. Boyd, J. C. Howell, *Phys. Rev. A* **2011**, *83*, 051803.
- [114] M. D'Angelo, F. V. Pepe, A. Garuccio, G. Scarcelli, *Phys. Rev. Lett.* **2016**, *116*, 223602.
- [115] F. Pepe, F. Di Lena, A. Garuccio, G. Scarcelli, M. D'Angelo, *Technologies* **2016**, *4*, 17.
- [116] F. V. Pepe, F. Di Lena, A. Mazzilli, E. Edrei, A. Garuccio, G. Scarcelli, M. D'Angelo, *Phys. Rev. Lett.* **2017**, *119*, 243602.
- [117] S. Dong, W. Zhang, Y. Huang, J. Peng, *Sci. Rep.* **2016**, *6*, 26022.
- [118] A. Stefanov, *Quantum Sci. Technol.* **2017**, *2*, 025004.
- [119] I. Afek, O. Ambar, Y. Silberberg, *Science* **2010**, *328*, 879.
- [120] J. W. Lichtman, J. A. Conchello, *Nat. Methods* **2005**, *2*, 910.
- [121] M. Renz, *Cytometry* **2013**, *83*, 767.
- [122] J. Jonkman, C. M. Brown, *J. Biomol. Tech.* **2015**, *26*, 54.
- [123] P. T. C. So, C. Y. Dong, B. R. Masters, K. M. Berland, *Annu. Rev. Biomed. Eng.* **2000**, *2*, 399.
- [124] D. I. Lee, T. Goodson, *J. Phys. Chem. B* **2006**, *110*, 25582.
- [125] H. W. D. Schlenk, in *Quantum Communications and Quantum Imaging XI* (Eds: R. E. Meyers, Y. Shih, K. S. Deacon) SPIE, Bellingham WA, USA **2013**.
- [126] J. P. Villabona-Monsalve, O. Calderin-Losada, M. Nuez Portela, A. Valencia, *J. Phys. Chem. A* **2017**, *121*, 7869.
- [127] O. Varnavski, B. Pinsky, T. Goodson, *J. Phys. Chem. Lett.* **2017**, *8*, 388.
- [128] F. Schlawin, *J. Phys. B: At., Mol. Opt. Phys.* **2017**, *50*, 203001.
- [129] F. Steinlechner, M. Gilaberte, M. Jofre, T. Scheidl, J. P. Torres, V. Pruneri, R. Ursin, *J. Opt. Soc. Am. B* **2014**, *31*, 2068.
- [130] M. Fiorentino, S. M. Spillane, R. G. Beausoleil, T. D. Roberts, P. Battle, M. W. Munro, *Opt. Express* **2007**, *15*, 7479.
- [131] S. M. Spillane, M. Fiorentino, R. G. Beausoleil, *Opt. Express* **2007**, *15*, 8770.
- [132] B. Dayan, A. Pe'er, A. A. Friesem, Y. Silberberg, *Phys. Rev. Lett.* **2004**, *93*, 023005.
- [133] B. Dayan, A. Pe'er, A. A. Friesem, Y. Silberberg, *Phys. Rev. Lett.* **2005**, *94*, 043602.
- [134] C. K. Hong, Z. Y. Ou, L. Mandel, *Phys. Rev. Lett.* **1987**, *59*, 2044.
- [135] H. Shin, K. W. C. Chan, H. J. Chang, R. W. Boyd, *Phys. Rev. Lett.* **2011**, *107*, 083603.
- [136] H. Lee, P. Kok, J. P. Dowling, *J. Mod. Opt.* **2002**, *49*, 2325.
- [137] A. N. Boto, P. Kok, D. S. Abrams, S. L. Braunstein, C. P. Williams, J. P. Dowling, *Phys. Rev. Lett.* **2000**, *85*, 2733.

- [138] T. Ono, R. Okamoto, S. Takeuchi, *Nat. Commun.* **2013**, *4*, 2426.
- [139] Y. Israel, S. Rosen, Y. Silberberg, *Phys. Rev. Lett.* **2014**, *112*, 103604.
- [140] A. Lyons, G. C. Knee, E. Bolduc, T. Roger, J. Leach, E. M. Gauger, D. Faccio, *Sci. Adv.* **2018**, *4*, eaap9416.
- [141] M. B. Nasr, B. E. Saleh, A. V. Sergienko, M. C. Teich, *Phys. Rev. Lett.* **2003**, *91*, 083601.
- [142] T. Meany, M. Grfe, R. Heilmann, A. Perez-Leija, S. Gross, M. J. Steel, M. J. Withford, A. Szameit, *Laser Photonics Rev.* **2015**, *9*, 363.
- [143] D. Grassani, S. Azzini, M. Liscidini, M. Galli, M. J. Strain, M. Sorel, J. E. Sipe, D. Bajoni, *Optica* **2015**, *2*, 88.
- [144] Y. H. Li, Z. Y. Zhou, Z. H. Xu, L. X. Xu, B. S. Shi, G. C. Guo, *Phys. Rev. A* **2016**, *94*, 043810.
- [145] Y. H. Li, Z. Y. Zhou, L. T. Feng, W. T. Fang, S. I. Liu, S. K. Liu, K. Wang, X. F. Ren, D. S. Ding, L. X. Xu, B. S. Shi, *Phys. Rev. Applied* **2017**, *7*, 064005.
- [146] A. Autere, H. Jussila, A. Marini, J. Saavedra, Y. Dai, A. Säynätjoki, L. Karvonen, H. Yang, B. Amirsoleimani, R. A. Norwood, N. Peyghambarian, H. Lipsanen, K. Kieu, F. J. G. de Abajo, Z. Sun, *Phys. Rev. B* **2018**, *98*, 115426.
- [147] Z. Y. Zhou, S. L. Liu, S. K. Liu, Y. H. Li, D. S. Ding, G. C. Guo, B. S. Shi, *Phys. Rev. Applied* **2017**, *7*, 064025.
- [148] I. Afek, O. Ambar, Y. Silberberg, *Science* **2010**, *328*, 879.
- [149] Y. M. Sua, H. Fan, A. Shahverdi, J. Y. Chen, Y. P. Huang, *Sci. Rep.* **2017**, *7*, 17494.
- [150] R. McCracken, F. Graffitti, A. Fedrizzi, arXiv:1807.00659 [quant-ph], **2018**.
- [151] B. Haase, M. Kutas, F. Rixinger, P. Bickert, A. Keil, D. Molter, M. Bortz, G. von Freymann, *Opt. Express* **2019**, *27*, 7458.
- [152] H. Danino, I. Freund, *Phys. Rev. Lett.* **1981**, *46*, 1127.
- [153] S. Schwartz, R. Coffee, J. Feldkamp, Y. Feng, J. Hastings, G. Yin, S. Harris, *Phys. Rev. Lett.* **2012**, *109*, 013602.
- [154] B. W. Adams, C. Buth, S. M. Cavaletto, J. Evers, Z. Harman, C. H. Keitel, A. Plffy, A. Picn, R. Rhlsberger, Y. Rostovtsev, K. Tamasaku, *J. Mod. Opt.* **2013**, *60*, 2.
- [155] R. H. Hadfield, *Nat. Photonics* **2009**, *3*, 696.
- [156] I. Gyongy, N. Calder, A. Davies, N. A. W. Dutton, R. R. Duncan, C. Rickman, P. Dalgarno, R. K. Henderson, *IEEE Trans. Electron Devices* **2018**, *65*, 547.
- [157] M. Perenzoni, N. Massari, D. Perenzoni, L. Gasparini, D. Stoppa, *IEEE J. Solid-State Circuits* **2016**, *51*, 155.
- [158] M. Perenzoni, D. Perenzoni, D. Stoppa, *IEEE J. Solid-State Circuits* **2017**, *52*, 151.
- [159] L. Gasparini, M. Zarghami, H. Xu, L. Parmesan, M. M. Garcia, M. Unternährer, B. Bessire, A. Stefanov, D. Stoppa, M. Perenzoni, in *IEEE International Conf. on Solid-State Circuits*, San Francisco, CA, February **2018**, pp. 98–100.
- [160] M. Unternährer, B. Bessire, L. Gasparini, D. Stoppa, A. Stefanov, *Opt. Express* **2016**, *24*, 28829.
- [161] L. Chen, D. Schwarzer, V. B. Verma, M. J. Stevens, F. Marsili, R. P. Mirin, S. W. Nam, A. M. Wodtke, *Acc. Chem. Res.* **2017**, *50*, 1400.
- [162] F. Marsili, F. Bellei, F. Najafi, A. E. Dane, E. A. Dauler, R. J. Molnar, K. K. Berggren, *Nano Lett.* **2012**, *12*, 4799.
- [163] C. Xiong, X. Zhang, Z. Liu, M. J. Collins, A. Mahendra, L. G. Helt, M. J. Steel, D. Y. Choi, C. J. Chae, P. H. W. Leong, B. J. Eggleton, *Nat. Commun.* **2016**, *7*, 10853.
- [164] N. Lusardi, J. W. N. Los, R. B. M. Gourgues, G. Bulgarini, A. Geraci, *Rev. Sci. Instrum.* **2017**, *88*, 035003.
- [165] C. Cahall, K. L. Nicolich, N. T. Islam, G. P. Lafyatis, A. J. Miller, D. J. Gauthier, J. Kim, in *2018 Conf. on Lasers and Electro-Optics*, San Jose, CA, May **2018**, pp. 1–2.
- [166] Q. Y. Zhao, D. Zhu, N. Calandri, A. E. Dane, A. N. McCaughan, F. Bellei, H. Z. Wang, D. F. Santavicca, K. K. Berggren, *Nat. Photonics* **2017**, *11*, 247.
- [167] Q. Zhao, A. McCaughan, F. Bellei, F. Najafi, D. De Fazio, A. Dane, Y. Ivry, K. K. Berggren, *Appl. Phys. Lett.* **2013**, *103*, 142602.
- [168] M. S. Allman, V. B. Verma, M. Stevens, T. Gerrits, R. D. Horansky, A. E. Lita, F. Marsili, A. Beyer, M. Shaw, D. Kumor, R. Mirin, S. W. Nam, *Appl. Phys. Lett.* **2015**, *106*, 192601.
- [169] B. Cabrera, R. Clarke, P. Colling, A. Miller, S. Nam, R. Romani, *Appl. Phys. Lett.* **1998**, *73*, 735.
- [170] A. E. Lita, A. J. Miller, S. W. Nam, *Opt. Express* **2008**, *16*, 3032.
- [171] B. M. Jost, A. V. Sergienko, A. F. Abouraddy, B. E. A. Saleh, M. C. Teich, *Opt. Express* **1998**, *3*, 81.
- [172] J. L. Blanchet, F. Devaux, L. Furfaro, E. Lantz, *Phys. Rev. Lett.* **2008**, *101*, 233604.
- [173] P. A. Moreau, J. Mougins-Sisini, F. Devaux, E. Lantz, *Phys. Rev. A* **2012**, *86*, 010101.
- [174] M. P. Edgar, D. S. Tasca, F. Izdebski, R. E. Warburton, J. Leach, M. Agnew, G. S. Buller, R. W. Boyd, M. J. Padgett, *Nat. Commun.* **2012**, *3*, 984.
- [175] P. A. Moreau, F. Devaux, E. Lantz, *Phys. Rev. Lett.* **2014**, *113*, 160401.
- [176] E. Lantz, S. Denis, P. A. Moreau, F. Devaux, *Opt. Express* **2015**, *23*, 26472.
- [177] R. Lin, A. Clowsley, D. Baddeley, I. Jayasinghe, C. Soeller, *Biophys. J.* **2016**, *110*, 161a.
- [178] F. Bleckmann, Z. Cherpakova, S. Linden, A. Alberti, *Phys. Rev. B* **2017**, *96*, 045417.
- [179] A. Ojaghi, M. E. Fay, W. A. Lam, F. E. Robles, *Sci. Rep.* **2018**, *8*, 9913.
- [180] D. S. Ding, Z. Y. Zhou, W. Huang, B. S. Shi, X. B. Zou, G. C. Guo, *Phys. Rev. A* **2012**, *86*, 033803.
- [181] J. S. Dam, P. Tidemand-Lichtenberg, C. Pedersen, *Nat. Photonics* **2012**, *6*, 788.
- [182] Z. Y. Zhou, Y. Li, D. S. Ding, Y. K. Jiang, W. Zhang, S. Shi, B. S. Shi, G. C. Guo, *Sci. Rep.* **2014**, *4*, 5650.
- [183] S. Junaid, S. C. Kumar, M. Mathez, M. Hermes, N. Stone, N. Shepherd, M. Ebrahim-Zadeh, P. Tidemand-Lichtenberg, C. Pedersen, *Optica* **2019**, *6*, 702.
- [184] S. K. Choi, M. Vasilyev, P. Kumar, *Phys. Rev. Lett.* **1999**, *83*, 1938.
- [185] P. M. Vaughan, R. Trebino, *Opt. Express* **2011**, *19*, 8920.
- [186] H. Rubinsztein-Dunlop, A. Forbes, M. V. Berry, M. R. Dennis, D. L. Andrews, M. Mansuripur, C. Denz, C. Alpmann, P. Banzer, T. Bauer, E. Karimi, L. Marrucci, M. Padgett, M. Ritsch-Marte, N. M. Litchinitser, N. P. Bigelow, C. Rosales-Guzmán, A. Belmonte, J. P. Torres, T. W. Neely, M. Baker, R. Gordon, A. B. Stilgoe, J. Romero, A. G. White, R. Fickler, A. E. Willner, G. Xie, B. McMorran, A. M. Weiner, *J. Opt.* **2016**, *19*, 013001.
- [187] F. Steinlechner, N. Hermosa, V. Pruneri, J. P. Torres, *Sci. Rep.* **2016**, *6*, 21390.
- [188] S. Kumar, H. Zhang, S. Maruca, Y. P. Huang, *Opt. Lett.* **2019**, *44*, 98.
- [189] B. Sephton, A. Vallés, F. Steinlechner, T. Konrad, J. P. Torres, F. S. Roux, A. Forbes, *Opt. Lett.* **2019**, *44*, 586.
- [190] A. P. Vandevender, P. G. Kwiat, *J. Mod. Opt.* **2004**, *51*, 1433.
- [191] M. A. Albota, F. N. Wong, *Opt. Lett.* **2004**, *29*, 1449.
- [192] L. Ma, O. Slattery, X. Tang, *Opt. Express* **2009**, *17*, 14395.
- [193] S. Ramelow, A. Fedrizzi, A. Poppe, N. K. Langford, A. Zeilinger, *Phys. Rev. A* **2012**, *85*, 013845.
- [194] M. Mancinelli, A. Trenti, S. Piccione, G. Fontana, J. S. Dam, P. Tidemand-Lichtenberg, C. Pedersen, L. Pavesi, *Nat. Commun.* **2017**, *8*, 15184.
- [195] H. Rütz, K. H. Luo, H. Suche, C. Silberhorn, *Phys. Rev. Appl.* **2017**, *7*, 024021.
- [196] Z. Y. Zhou, Y. Li, D. S. Ding, W. Zhang, S. Shi, B. S. Shi, G. C. Guo, *Light: Sci. Appl.* **2016**, *5*, e16019.
- [197] L. Mertens, M. Sonnleitner, J. Leach, M. Agnew, M. J. Padgett, *Sci. Rep.* **2017**, *7*, 42164.

- [198] D. Shin, F. Xu, D. Venkatraman, R. Lussana, F. Villa, F. Zappa, V. K. Goyal, F. N. Wong, J. H. Shapiro, *Nat. Commun.* **2016**, *7*, 12046.
- [199] S. Shi, A. Thomas, N. V. Corzo, P. Kumar, Y. Huang, K. F. Lee, *Sci. Rep.* **2016**, *6*, 24344.
- [200] X. Zhao, J. Cheng, Q. Xiong, L. Hua, G. Jiang, *Appl. Opt.* **2018**, *57*, 5623.
- [201] S. Signorini, M. Mancinelli, M. Borghi, M. Bernard, M. Ghulinyan, G. Pucker, L. Pavesi, *Photon. Res.* **2018**, *6*, 805.
- [202] K. Rottwitz, J. G. Koefoed, E. N. Christensen, *Fibers* **2018**, *6*.